Transcription Machinery Anchors ecDNAs to Mitotic Chromosomes for Segregation

Yipeng Xie[1], Jun Yi Stanley Lim[1], Wenyue Liu[2], Collin Gilbreath[1], Yoon Jung Kim[1*], Sihan Wu[1*]

[1] Children's Medical Center Research Institute, University of Texas Southwestern Medical Center, Dallas, TX, USA.

[2] Department of Cell Biology, University of Texas Southwestern Medical Center, Dallas, TX, USA.

* Corresponding authors.

Abstract

Extrachromosomal DNA (ecDNA) is a prevalent driver of cancer, whose random segregation promotes aggressive tumors. Acentric ecDNAs attach to chromosomes during mitosis for segregation. However, the molecular mechanism governing ecDNA-chromosome mitotic interactions remains poorly understood. This study shows that ecDNAs attach to histone 3 lysine 27 acetylation (H3K27ac)-marked chromatin during mitosis. H3K27ac depletion resulted in ecDNA detachment from mitotic chromosomes. Diverse bromodomain proteins, which are known readers of H3K27ac, stabilize ecDNAs' mitotic interaction, exhibiting context-dependent and mutually complementary roles. Furthermore, disruptions of the Mediator complex and RNA polymerase II transcription activity both dissociate ecDNAs from mitotic chromosomes, suggesting that the transcription machinery mediates ecDNA segregation. Mis-segregated ecDNAs were expelled into the cytosol and degraded, leading to diminished oncogene expression and a reversal of therapy resistance. Our research provides new insights into the interplay between RNA transcription and acentric ecDNA inheritance in cancer, offering a novel avenue for disrupting ecDNA-driven oncogenesis.

Introduction

DNA transmission to daughter cells during cell division is a fundamental process in inheritance, ensuring the stability of genetic information across generations.[1] In eukaryotes, chromosomal inheritance involves spindle fiber attachment to the kinetochore at the centromere, which facilitates the equal distribution of chromosomes between two daughter cells.[2,3] However, the inheritance mechanism for acentric extrachromosomal DNA (ecDNA), a prevalent oncogene carrier in aggressive tumors, remains unclear.

ecDNA is chromatinized circular DNA specifically found in cancer with a typical size ranging from 50-kb to 5-Mb.[4] It is present in nearly half of all human cancer types and up to one-third of cancer patients throughout their disease.[5–7] ecDNA carries diverse oncogenes, immunoregulatory genes, and associated enhancers.[8,9] Owing to high copy numbers and hyper-accessible chromatin, ecDNA can drive massive oncogene expression.[10] More importantly, a lack of functional centromeres cause ecDNAs to segregate randomly during cancer cell division, similar to plasmid inheritance in bacteria.[11–14] This random distribution generates a heterogeneous pool of cancer cells with varying oncogene copy numbers in every cell cycle. In several cancer types, including small cell lung cancer, glioblastoma, and medulloblastoma, ecDNA's asymmetric segregation has been shown to promote rapid tumor evolution, stress adaptation, and therapy resistance.[15–17] In addition, a recent study has demonstrated that distinct ecDNA species within a single cell can co-segregate into daughter cells.[18] Such behavior further enables ecDNA to evade the Mendelian inheritance principles and foster tumor aggressiveness. Thus, revealing

37 the molecular mechanism mediating ecDNA segregation is critical for understanding cancer
38 genome maintenance and developing effective therapeutic strategies for ecDNA-driven cancers.

39 How do ecDNAs segregate during mitosis? Historically, it was proposed that ecDNAs attach to
40 chromosomes for segregation as early as 1978.[19] Subsequent imaging studies have confirmed
41 this finding, showing that ecDNAs hitchhike on mitotic chromosomes during cell division.[13,20,21]
42 However, the intricate molecular mechanism underlying such mitotic interaction between
43 ecDNAs and chromosomes has not been elucidated.

44 The tethering of ecDNAs to mitotic chromosomes represents a unique form of chromatin-
45 chromatin interaction. The negatively charged DNA backbone, due to its phosphate groups,
46 suggests that local chromatin modifications and binding proteins are necessary to mediate
47 ecDNA-chromosome interactions during mitosis, overcoming the inherent electrostatic repulsion
48 between DNA molecules. The present study aims to investigate the histone modifications and
49 protein complexes that facilitate ecDNA segregation, thereby providing new insights into the
50 mechanism of oncogenic inheritance in cancer.

51

52 Results

53 1. ecDNA trans-interaction sites on mitotic chromosomes are enriched with 54 H3K27ac and H3K4me3 chromatin

55 We previously demonstrated that, even during metaphase, ecDNA chromatin is enriched with
56 active histone modifications (Figure S1A), including H3K27ac and H3K4 tri-methylation
57 (H3K4me3), and a paucity of repressive histone marks.[10] In addition, ecDNAs may interact with
58 chromosomes via their active chromatin in an enhancer-promoter contact fashion.[22] This
59 prompted us to investigate whether H3K27ac and H3K4me3, which mark active enhancers and
60 promoters, are required for ecDNA segregation. We used the MSTO211H lung cancer cell line
61 as our model system and performed *in situ* HiC to profile ecDNA trans-interaction sites during
62 mitosis and correlated them with H3K27ac and H3K4me3 CUT&RUN data (Figure 1A, Figure
63 S1B). Mitotic cells were enriched with nocodazole treatment and sorted for the phosphorylated
64 MPM2-positive and 4N DNA content fraction.[23] The MPM2-negative, 2N DNA content fraction
65 representing the G1 phase cells was sorted as control (Figure 1A). The MSTO211H cell line
66 carries *MYC* ecDNAs made of a simple structure originating from a 500-kb DNA segment of
67 chromosome 8, enabling us to distinguish ecDNA trans-interaction from DNA translocation
68 (Figure 1B, Figure S1C).

69 Over 600 million valid HiC interaction pairs per library were obtained, with high reproducibility
70 between replicates (Figure S1D-E). Compared to the G1 phase, topologically associating
71 domains were largely reduced in agreement with previous reports.[24,25] ecDNA-derived global
72 trans-interactions were also detected as previously observed but notably decreased at the M

phase (Figure 1C-D), suggesting fewer chromatins from mitotic chromosomes remained accessible for ecDNA to interact with.

Next, we interrogated the association of ecDNA trans-interaction sites with active histone marks. To maximize the resolution, we merged replicates for each cell cycle fraction and identified trans-interactions at a 10-kb resolution. Significant trans-interactions were defined as the top 0.1% of ecDNA contacts with non-ecDNA-originated chromosomes, excluding chromosome 8, where *MYC* ecDNAs originated (Figure S1F), yielding 584 significant ecDNA trans-interaction sites during mitosis. Compared to 1,000 randomly selected 10-kb genomic intervals, ecDNA trans-interaction sites during mitosis were enriched with H3K27ac and H3K4me3 marks, as evidenced by higher sequencing coverage and read counts of these histone marks within the ecDNA trans-interaction sites (Figure 1E-F, Figure S1G). These data suggest that ecDNAs may be preferentially associated with active chromatin regions during segregation.

2. H3K27ac is essential for ecDNA tethering to mitotic chromosomes

H3K27ac is mainly enriched at active enhancers and promoters.[26] We first used A485, an acetyl-CoA competitive CBP/P300 inhibitor,[27] to deplete H3K27ac and study whether ecDNAs were detached from mitotic chromosomes (Figure 2A-B). When H3K27ac was globally decreased as measured by CUT&RUN in MSTO211H cells, *MYC* ecDNAs were significantly detached from chromosomes during metaphase (Figure 2C-E). This observation was independently verified in SNU16 stomach cancer cells with *MYC* and *FGFR2* ecDNAs and COLO320DM colon cancer cells with *MYC* ecDNAs (Figure S2A-F), suggesting that H3K27ac is commonly required for ecDNA interaction with mitotic chromosomes.

We employed two strategies to further validate the involvement of H3K27ac. First, we used a histone deacetylase inhibitor, SAHA,[28] to counteract the effect of A485. When MSTO211H cells were treated with SAHA and A485, H3K27ac modification was rescued similarly to the control level (Figure 2C, Figure S2G-H). In the meantime, *MYC* ecDNAs' association with mitotic chromosomes was also recovered (Figure 2D-E). Next, we used RNAi to knockdown CBP and P300, the writers of H3K27ac,[29] and observed the same ecDNA detachment phenotype as the A485 treatment (Figure 2F-H). These data collectively show that H3K27ac is an essential histone modification for ecDNA segregation.

We then tested whether H3K4me3, which marks active promoters,[30] is required for ecDNA-chromosome mitotic interaction. H3K4 methylation is deposited by the COMPASS complex, which contains diverse methyltransferases from the SET1 and MLL family and shared subunits, including DPY30 and RBBP5.[31,32] Global H3K4me3 level was downregulated when DPY30 and RBBP5 were knocked down by RNAi (Figure S2I). However, neither *MYC* nor *FGFR2* ecDNAs were detached from mitotic chromosomes in SNU16 cells (Figure S2J-K), suggesting that H3K4me3 does not mediate ecDNA segregation.

3. Diverse bromodomain proteins anchor ecDNAs to mitotic chromosomes

While H3K27ac is shown to facilitate ecDNA segregation, it does not fully explain why ecDNA-chromosome interaction becomes feasible because the acetyl group is not sufficient to neutralize the negative charge of the DNA backbone. Thus, we hypothesized that proteins bound to H3K27ac chromatin are necessary to mediate ecDNA mitotic interaction with chromosomes.

Bromodomain-containing proteins are well-known as readers of H3K27ac chromatin.[33] We analyzed the RNA expression levels of all 40 human bromodomain proteins in common ecDNA-containing cancer cell lines, using RNA-seq data from DepMap and other public datasets.[10,34] The most highly expressed genes belong to two families, the bromodomain and extraterminal (BET) protein family, including BRD2, BRD3, and BRD4, and the SWI/SNF complexes, including SMARCA2/4 and BRD7/9 (Figure 3A, Figure S3A). This prompted us to study whether BET or SWI/SNF proteins are involved in ecDNA segregation.

When BET proteins in SNU16 cells were degraded by a PROTAC molecule dBET6, which comprises a JQ1 structure conjugated to a cereblon E3 ubiquitin ligase ligand,[35] both *MYC* and *FGFR2* ecDNAs were effectively detached from mitotic chromosomes (Figure 3B-C, Figure S3B). Pan-BET protein degradation achieved a similar effect in COLO320DM cells, in which *MYC* ecDNAs were also detached during metaphase (Figure S3C-E).

However, when individual BET genes were knocked down, including highly expressed BRD2 and BRD4 and relatively lower abundant BRD3, we did not observe a significant dissociation of *MYC* or *FGFR2* ecDNAs from mitotic chromosomes in SNU16 cells, even though over 75% transcripts were depleted (Figure S3F-H). Among all BET proteins, BRD4 is a known regulator for *MYC* ecDNA hub formation and gene expression in COLO320DM cells.[36] However, when the BRD4 protein was effectively degraded by dTAGv1 through an endogenously knock-in FKBP12^{F36V} degron, we did not observe a significant *MYC* ecDNA detachment in COLO320DM cells (Figure S3I-K). These data suggest that BET proteins act collaboratively in an interchangeable fashion.

The interchangeability of bromodomain proteins motivated us to investigate whether BET proteins serve as a universal factor in anchoring ecDNAs to mitotic chromosomes. In MSTO211H cells, treatment with dBET6 resulted in the effective degradation of BET proteins, as exemplified by BRD4 depletion. However, *MYC* ecDNAs remained associated with chromosomes during metaphase (Figure 3D-F). Similarly, the treatment with a SMARCA2/4 PROTAC molecule AU15330[37] did not detach ecDNAs (Figure 3D-F). In contrast, concurrent inhibition of both BET proteins and SWI/SNF complex via treatment with dBET6 and AU15330 resulted in a significant dissociation of *MYC* ecDNAs with mitotic chromosomes in MSTO211H cells (Figure 3G-H). Collectively, these results indicate that various bromodomain proteins participate in the segregation of ecDNA, functioning in a context-dependent and interchangeable way.

147

148 ## 4. Mediator complex is required for ecDNA segregation

149 BET and SWI/SNF proteins have been established as critical regulators of enhancer-promoter
150 interactions, facilitating the assembly of the transcription machinery through their interactions
151 with the Mediator complex.[38,39] We then investigated whether the Mediator is also involved in
152 ecDNA segregation.

153 The core Mediator is a large, multi-subunit complex whose functional activity is regulated by its
154 kinase module, which includes cyclin-dependent kinases, notably CDK8 (Figure 4A).[40] When
155 CDK8 was knocked down by RNAi, ecDNAs in MSTO211H and SNU16 cells were significantly
156 detached from mitotic chromosomes (Figure 4B-D, Figure S4A-C). This finding suggests a
157 pivotal role for the Mediator complex in the segregation of ecDNAs during cell division.
158 Furthermore, the dependence of this mechanism on CDK8's kinase activity was confirmed by
159 the results of Cyclin C knockdown, an essential regulator for CDK8 activation, which similarly
160 resulted in the detachment of ecDNAs in both cell lines (Figure 4E-F, Figure S4A-C).

161 Next, we interrogated whether CDK8 regulates ecDNA segregation through the Mediator
162 complex. The core Mediator complex lacks transcriptional competence when associated with
163 the kinase module.[38,41] The degradation of MED13, another subunit of the kinase module,
164 liberates the CDK8-containing kinase module from the core Mediator complex, thereby
165 facilitating the interaction between the Mediator and the RNA polymerase II preinitiation complex,
166 which is essential for transcription initiation.[42,43] Based on this understanding, we hypothesized
167 that the absence of MED13 would enable ecDNAs to interact with mitotic chromosomes
168 independently of CDK8. Upon the knockdown of *MED13*, we observed a significant rescue of
169 ecDNA dissociation caused by CDK8 knockdown (Figure 4G-I). Collectively, these results
170 indicate that the Mediator complex is crucial for the tethering of ecDNAs to mitotic chromosomes.

171

172 ## 5. ecDNA segregation is coupled with mitotic transcription activity

173 The involvement of bromodomain proteins and the Mediator complex suggests that the
174 transcription machinery may engage in the ecDNA segregation process. Therefore, we used
175 various transcription inhibitors to study whether mitotic transcription activity is required for
176 tethering ecDNAs to chromosomes during mitosis (Figure 5A-B).

177 A 6-hour treatment of triptolide, actinomycin D, or α-amanitin successfully inhibited RNA
178 polymerase II transcription activity, as exemplified by the decrease of total polymerase II protein
179 abundance and its phosphorylation on the serine 2/5 residues (Figure S5A). Using qPCR to
180 measure the level of *MYC* mRNA, whose half-life was reported to be only 10-30 min,[44] we also
181 found a dramatic reduction in the transcription activity after inhibitor treatments (Figure S5B).

And when the transcription activity was suppressed, *MYC* ecDNAs in MSTO211H cells were profoundly detached from mitotic chromosomes (Figure 5C-E).

This phenomenon was not confounded by the deficit of other proteins necessary to tether ecDNAs because of transcription inhibition. First, critical ecDNA segregation proteins, such as SMARCA4 and CDK8, did not markedly decrease under such dosage and duration of transcription inhibitor treatments in MSTO211H cells (Figure S5C); only BRD4 was partially affected, which was not sufficient to cause ecDNA detachment in this cell line, as shown above (Figure 3D-F). Second, when protein synthesis was inhibited during mitosis with a 2-hour cycloheximide treatment, which effectively abolished nascent protein production, *MYC* ecDNAs' interaction with mitotic chromosomes was maintained (Figure S5D-F). Taken together, these data clearly support that mitotic transcription is essential for ecDNA segregation.

6. Mis-segregated ecDNAs are expelled to the cytosol

We further explored the outcomes of mis-segregated ecDNAs. We took advantage of an engineered COLO320DM cell line with TetO array inserted into their *MYC* ecDNA, which can be visualized with TetR-mNeonGreen using time-lapse live-cell microscopy.[36] When these cells were treated with dBET6 to degrade BET proteins and induce ecDNA detachment from mitotic chromosomes, mis-segregated ecDNAs were excluded from the primary nuclei in the following cell cycle, forming micronuclei in the cytosol (Figure 6A). This phenomenon was independently validated in SNU16 cells by fixed-cell imaging. When cells were treated with A485 to inhibit H3K27ac and FISH for ecDNAs after one cell cycle, we found a significant increase in cytosolic FISH signals, suggesting that mis-segregated ecDNAs were expelled to the cytosol of interphase cells in the next cell cycle (Figure S6A-B).

ecDNA mis-segregation led to its depletion. A long-term A485 treatment in MSTO211H gradually eliminated the number of ecDNA over 3 weeks and, eventually, diminished the expression of ecDNA-borne oncogenes, such as *MYC* (Figure 6B-C, Figure S6C). We then asked whether ecDNA depletion could inhibit cancer aggressiveness, such as therapy resistance. We employed the HeLa-ecDHFR model, in which *DHFR* ecDNAs were induced and maintained by long-term exposure to methotrexate.[45] Degradation of BET proteins by dBET6 also induced *DHFR* ecDNA mis-segregation (Figure 6D-E, Figure S6D). While the removal of methotrexate decreased *DHFR* ecDNAs in agreement with previous studies,[46] dBET6 treatment accelerated the loss of *DHFR* ecDNAs (Figure 6F). Consequently, ecDNA-depleted HeLa cells were re-sensitized to methotrexate (Figure 6G).

In summary, these data show that mis-segregated ecDNAs were expelled into the cytosol, resulting in the loss of ecDNAs. Depletion of ecDNAs decreases ecDNA-borne oncogene expression and can re-sensitize cancer cells to therapy, whose resistance is driven by ecDNA.

Discussion

The random segregation of acentric ecDNAs represents a crucial driver of tumor evolution.[15–17] This process leads to the unequal distribution of ecDNA particles among daughter cells during cell division, thereby fostering tumor heterogeneity. As a result, a diverse pool of cancer cells emerges, each processing varied oncogene copy numbers that facilitate rapid adaptation to the dynamic tumor microenvironment, particularly under therapeutic pressure.[13]

While previous research has suggested that chromosome hitchhiking mediates ecDNA segregation, the precise molecular mechanism governing the interaction between ecDNAs and chromosomes during mitosis remains poorly characterized. We propose a model in which ecDNAs attach to mitotic chromosomes via H3K27ac-marked active chromatin interaction. This interaction is mediated by the transcription machinery comprising bromodomain proteins, the Mediator complex, and RNA polymerase II. While half of the chromatin-bound RNA polymerase II is dissociated from chromosomes during mitosis as compared to interphase,[47] ecDNAs remain transcriptionally active during mitosis as shown by nascent RNA FISH, which is required for ecDNA aggregation and co-segregation into daughter cells.[18] These findings collectively suggest that the inheritance of ecDNA is intrinsically linked to its transcription.

Our finding further emphasizes that mis-segregated ecDNAs are expelled into the cytosol and gradually depleted, leading to the loss of oncogene expression and therapy resistance. This finding opens a new avenue for treating ecDNA-driven cancer by targeting ecDNA segregation. Within the ecDNA segregation machinery, many targets are considered actionable. For example, small molecules targeting histone lysine acetyltransferases, bromodomain proteins, and CDK8 are currently under investigation in clinical trials.[48–51] Future studies should aim to elucidate whether patients with ecDNA-containing tumors will derive therapeutic benefit from these strategies.

Moreover, our study identifies H3K27ac, the Mediator complex, and RNA polymerase II as universal adapters that anchor ecDNAs to mitotic chromosomes. However, we also observe that bromodomain proteins exhibit mutually complementary roles, contingent upon the specific cancer model examined. Notably, in the MSTO211H cancer cell with *MYC* ecDNAs, the degradation of both BET and SWI/SNF proteins was necessary to disrupt ecDNA segregation. This finding raises a critical question regarding whether the segregation of ecDNA is influenced by the specific bromodomain proteins that regulate the expression of its cargo gene.

An intriguing aspect of our findings is that, even with no perturbations, ecDNA segregation is “leaky” in a few cells, where certain ecDNA particles are not consistently attached to mitotic chromosomes. This phenomenon may lead to the accumulation of cytosolic DNA in ecDNA-driven cancer, which may trigger innate immunity sensing pathways, such as the cGAS/STING

pathway.[52] Although many cancers have evolved mechanisms to silence the expression of cGAS or STING, the relationship between the deactivation of these pathways and ecDNA pathogenesis warrants further investigation.[53] Alternatively, it is also important to understand whether cancer may hijack this pathway for chronic STING activation and promote its growth and metastasis.[1]

One limitation of this study regards the dynamic alteration of H3K27ac during mitosis and its potential impact on the HDAC of the transcription machinery. H3K27ac is significantly diminished at promoters and enhancers during prometaphase and quickly re-emerged during anaphase and telophase.[54,55] However, certain regions retain H3K27ac during mitosis, including the promoters of housekeeping genes and enhancers associated with cell identity genes in stem cells.[56] This phenomenon of mitotic bookmarking is essential for transcriptional memory across cell division.[57,58] Future studies should explore whether ecDNAs interact with these bookmarking gene loci to facilitate their segregation, which may yield further insights into the complexities of ecDNA behavior during mitosis.

Methods

Cell culture

MSTO211H, SNU16, and COLO320DM cells were obtained from ATCC. All cells were cultured in Dulbecco's Modified Eagle's Medium/F12 (DMEM/F12; Corning) supplemented with 10% Fetal Bovine Serum (FBS; Corning) and 1× Penicillin-Streptomycin (Corning), maintained at 37°C in a humidified incubator with 5% CO_2, and regularly tested for mycoplasma. The HeLa-ecDHFR cell line was a gift from Dr. Roel Verhaak, which carries artificially induced *DHFR* ecDNA by long-term exposure to methotrexate. To maintain *DHFR* ecDNAs, 20 μM methotrexate was added to the cell culture media. The COLO320DM TetO-MYC TetR-mNeonGreen cell line[36] was a gift from Dr. Paul Mischel, with its ecDNA inserted with a TetO array and labeled with stably expressed TetR-mNeonGreen. The COLO320DM-BRD4::FKBP12^{F36V} cell line was generated by inserting the FKBP12^{F36V} sequence into the C-terminus of the *BRD4* endogenous locus using CRISPR-Cas9.

Enrichment of metaphase and anaphase cells

Cells were seeded overnight on glass coverslips coated with Poly-D-Lysine (PDL; Sigma-Aldrich). Prophase and prometaphase cells were arrested with 100 ng/ml nocodazole (Sigma-Aldrich) for 12-16 hr at 37°C. After arrest, cells were washed 3× with pre-warmed PBS and released in growth media for 40-50 min at 37°C, allowing them to progress to metaphase and anaphase. The following compounds were added before or during the nocodazole treatment, whose dosage and timing were indicated in the corresponding main figures: A485 (Selleck Chemicals); dBET6 (Selleck Chemicals); AU-15330 (Medchemexpress); Actinomycin D (Selleck

289 Chemicals); Triptolide (Selleck Chemicals); α-amanitin (Santa Cruz Biotechnology);
290 Cycloheximide (Selleck Chemicals).

291 **Flow cytometry and sorting**

292 Single-cell suspensions were cross-linked with 2% formaldehyde (Sigma-Aldrich) for 10 min,
293 quenched with 0.3 M glycine (Sigma-Aldrich) for 10 min, and permeabilized with 0.1% saponin
294 (Thermo Scientific) in PBS for 10 min. After blocking with 1% FBS + 0.1% saponin for 30 min,
295 the anti-MPM2 (Sigma-Aldrich 05-368, 1:1,000) primary antibody was added to the blocking
296 solution and incubated for 1 hr. Cells were then washed 3× with PBS containing 0.1% saponin
297 before AlexaFluor-conjugated secondary antibodies (Invitrogen) staining for another 1 hr. After
298 another 3x washes, DNA was stained with 1 μg mL^{-1} DAPI for 5 min. Finally, cells were sorted
299 using the FACSAria Fusion (BD Biosciences) for G1 (2N DNA, MPM2-negative) and M phase
300 (4N DNA, MPM2-positive). All procedures were performed at room temperature (RT).

301 ***In situ* HiC**

302 *In situ* HiC libraries for G1 and M phases sorted cells were prepared with the Arima HiC kit (Arima
303 Genomics) following the manufacturer's instructions. In brief, one million sorted cells, which were
304 cross-linked with 2% formaldehyde before sorting, were digested with two restriction enzymes,
305 followed by end filling, biotin labeling, and proximal ligation. Next, 1.5 μg ligated DNA was
306 fragmentized by the Covaris ME220 (peak power: 75W; duty factor, 20%; cycles per burst: 200;
307 treatment time, 3.5 minutes) for 300-bp size selection with DNA purification beads. Biotin-labeled
308 DNA was then enriched with streptavidin beads for sequencing library preparation using the
309 Arima library prep module. HiC libraries were then pooled and sequenced with the paired-end
310 150 mode.

311 Adapter sequences were trimmed by the fastp software (v0.22.0). Trimmed reads were then
312 processed through the HiC-Pro pipeline (v3.1.0) with hg38 as the reference genome. The
313 reproducibility of HiC libraries was analyzed by the HiCRep software (v0.2.6). HiC interaction
314 was detected by the FitHiC2 software (v2.0.8).

315 **CUT&RUN sequencing**

316 CUT&RUN libraries were generated with the CUTANA ChIC/CUT&RUN kit version 4 (EpiCypher,
317 12-1048) and the CUT&RUN library prep kit (EpiCypher, 14-1001&14-1002) according to their
318 instructions. MSTO211H cells were cultured and treated as described above in 10-cm plates.
319 Cells were harvested by trypsinization and counted with Countess 3 Automated Cell counter
320 (Invitrogen). For one CUT&RUN sample preparation, 0.5 million cells were used to isolate nuclei
321 using the CUTANA Pre-Nuclei Extraction Buffer (EpiCypher, 21-1026a). Nuclei were then bound
322 to beads and incubated with 0.5 μg antibodies overnight. The following antibodies were used:
323 IgG (EpiCypher 13-0042), H3K4me3 (EpiCypher 13-0041), and H3K27ac (EpiCypher 13-0059).

Target DNAs bound by antibody were digested with pAG-MNase for 2 hours at 4°C and extracted by incubating with stop master mix containing 0.5 ng of E. coli Spike-in DNA at 37°C.

CUT&RUN sequencing data were analyzed as previously described.[59] In brief, sequencing data were aligned to the hg38 human genome. Unmapped and discordant read pairs were removed. The coverage was normalized with the spike-in control, which was determined by the abundance of reads aligned to the *Escherichia coli* genome.

RNA interference

Forty nanomolar respective siRNAs were mixed with Lipofectamine RNAiMAX Transfection Reagent (Invitrogen) following the manufacturer's instructions and incubated for 10 min at RT to form siRNA-lipid complexes. siRNA-lipid complexes were added dropwise into cell culture and gene knockdown was determined 48 hr after transfection. Information on siRNAs is provided in Supplementary Table S1.

DNA FISH

Cells on coverslips were rinsed with PBS and fixed using fresh Carnoy's fixative (3:1 methanol:acetic acid) for 10 min. Fixed cells were air-dried for 2 hr at room temperature or overnight at 4°C. Samples were equilibrated with 2× SSC and dehydrated in 70%, 85% and 100% ethanol for 2 min each. FISH probes (Empire Genomics) diluted in hybridization buffer (1:10) were applied to coverslips and mounted onto glass slides. Slides were denatured for 2 min at 75°C and hybridized overnight at 37°C in a humidified chamber. After removing from slides, coverslips were washed 2× in 0.4× SSC with 0.3% IGEPAL for 5 min, followed by another wash in 2× SSC with 0.1% IGEPAL for 5 min. DNA was counterstained with 1 μg mL^{-1} DAPI in 2× SSC for 5 min and washed 2× with 2× SSC for 5 min. Coverslips were mounted onto glass slides with VECTASHIELD antifade mounting medium (Vector Laboratories) and sealed for imaging. All procedures were performed at RT unless indicated otherwise.

Cytospin and immunofluorescence

Cells were arrested to metaphase with 33 ng/ul KaryoMAX colcemid (Gibco) overnight at 37°C and pelleted in hypotonic buffer (10 mM Tris-Cl (pH 7.5) + 20 mM NaCl + 5 mM KCl + 1 mM $CaCl_2$ + 0.5 mM $MgCl_2$ + 40 mM glycerol) for 15 min on ice. 0.1% Tween-20 was then added to the hypotonic buffer to permeabilize cells. Cells were deposited onto glass slides using Cytospin 4 Cytocentrifuge (Epredia) at 500 RPM for 10 min. Slides were aged overnight at 4°C and blocked with Renaissance background reducing diluent (Biocare Medical) for 10 min at RT. The following primary antibodies were diluted in the diluent and incubated for 1 hr at RT: anti-H3K27ac 1:100 (Cell Signaling Technology 8173S) and anti-H3K4me3 1:100 (Cell Signaling Technology 9751S). Slides were washed 3× with the diluent containing 0.1% Tween-20 for 5 min before AlexaFluor-conjugated secondary antibody staining (Invitrogen) for 1 hr at RT. Following another 3× washes as above, 1 μg mL^{-1} DAPI in the diluent was applied for DNA counterstaining.

360 Cells were then fixed with 4% formaldehyde for 15 min at RT before being mounted with
361 VECTASHIELD antifade mounting medium and sealed for imaging.

362 **Protein synthesis assay**

363 Cells on coverslips were treated with 5 μg/mL cycloheximide (Selleck Chemicals) for 2 hr.
364 Nascent protein synthesis was detected using the Click-&-Go Plus OPP protein synthesis assay
365 kit (Vector Laboratories) following the manufacturer's instructions. In brief, cells were labeled
366 with O-propargyl-puromycin (OPP) reagent after cycloheximide treatment. Cells were then fixed
367 with formaldehyde and permeabilized with 0.5% Triton X-100. After washing, the samples were
368 incubated with the reaction cocktail prepared according to the instructions and stained with 5
369 μg/mL Hoechst 33342. The slides were then mounted and imaged.

370 **Fluorescence microscopy**

371 DNA FISH, immunofluorescence, and protein synthesis assays were imaged on the Zeiss Axio
372 Observer 7 microscope equipped with the Apotome 3 optical sectioning module. Images were
373 acquired with a 63× Plan-Apochromat 1.40 NA oil objective and processed using ZEN software
374 (v3.4, Zeiss). At least five z-stacks were taken with an interval of 1 μm.

375 For live-cell imaging, COLO320DM TetO-MYC TetR-mNeonGreen cells were seeded in 35-mm
376 glass bottom dishes and treated with dBET6. Culture media were replaced with warm FluoroBrite
377 DMEM (Gibco) before imaging. Images were acquired with the Zeiss LSM 980 microscope
378 through a 63× oil objective. Three slices per 1 μm interval were recorded.

379 **Immunoblotting**

380 Cells were lysed in RIPA buffer supplemented with 1× protease inhibitor cocktail (Sigma-Aldrich)
381 and 1× phosphatase inhibitor cocktail (Sigma-Aldrich). To improve histone extraction efficiency,
382 lysates were added with 100 units μL^{-1} of Micrococcal Nuclease (New England Biolabs) and 1
383 mM calcium chloride and incubated for 15 min at RT. Lysates were then cleared by centrifugation
384 (17000 RCF for 15 min at 4°C) and quantified using Pierce Rapid Gold BCA Protein Assay Kit
385 (Thermo Scientific). Samples were resolved by SDS polyacrylamide gel electrophoresis and
386 transferred onto 0.2 μm nitrocellulose membranes (Bio-Rad). Membranes were blocked with 2%
387 Bovine Serum Albumin (BSA) in TBST (0.1% Tween-20 in TBS) for 1 hr at RT. The following
388 primary antibodies were diluted in 2% BSA in TBST and incubated with membranes overnight at
389 4°C: anti-BRD2 1:1,000 (Bethyl Laboratories A302-583A), anti-BRD3 1:1,000 (Bethyl
390 Laboratories A700-069), anti-BRD4 1:1,000 (Bethyl Laboratories A301-985A), anti-SMARCA4
391 1:1,000 (Cell Signaling Technology 49360S), anti-H3K27ac 1:1,000 (Cell Signaling Technology
392 8173S), anti-H3K4me3 1:1,000 (Cell Signaling Technology 9751S), anti-RPB1 1:1,000 (Cell
393 Signaling Technology 2629S), anti-phospho-RPB1 Ser2/5 1:1,000 (Cell Signaling Technology
394 13546S), anti-c-MYC 1:2,000 (Abcam ab32072), anti-HA tag 1:2,000 (Cell Signaling Technology
395 3724S), and anti-GAPDH 1:10,000 (Proteintech 60004-1-Ig). After primary antibody incubation,

396 membranes were washed 3× with TBST and incubated with HRP-conjugated secondary
397 antibodies (Cell Signaling Technology) diluted to 1:5,000 with 2% BSA in TBST for 1 hr at RT.
398 Membranes were washed 3× with TBST, developed using SuperSignal West Pico PLUS
399 Chemiluminescent Substrate (Thermo Scientific), and imaged using ImageQuant 800
400 (Amersham).

401 **qPCR**

402 For mRNA reverse transcription qPCR, RNA was extracted using the Quick-RNA Miniprep Plus
403 Kit (Zymo Research) and quantified by NanoDrop (Thermo Scientific). 1 µg RNA was reverse
404 transcribed to cDNA using the Maxima H Mirus reverse transcriptase (Thermo Scientific). 10 ng
405 cDNA was added with 1× SYBR Green qPCR Master Mix (Selleck Chemicals) and 400 nM
406 respective forward and reverse primers for qPCR on CFX Opus 96 System (Bio-Rad). The
407 relative RNA level was calculated by the ddCt method. The *TBP* transcript was used as a control
408 for most assays, except for the transcription inhibitor assessment, in which the long half-life
409 *RPL13A* transcript was used.

410 For DNA copy number qPCR, genomic DNA was extracted using the Quick-DNA Miniprep Plus
411 Kit (Zymo Research) and quantified by the Qubit assay (Thermo Scientific). 10 ng DNA was
412 added with 1× SYBR Green qPCR Master Mix (Selleck Chemicals) and 400 nM respective
413 forward and reverse primers for qPCR on CFX Opus 96 System. The gene copy number was
414 determined using *HBB* as a diploid control. Primer sequences are listed in Supplementary Table
415 S1.

416 **Cell viability assay**

417 5,000 cells/well HeLa-ecDHFR were seeded into 96-well plates. Cells were treated with
418 methotrexate for 4 days.10 µL CCK-8 reagents (Apexbio Technology) were added and incubated
419 at 37°C for 2 hr. Cell viability was determined as the absorbance at 450 nm using a plate reader.

420 **Statistics**

421 All statistical methods are indicated in the corresponding figure legends. Student's t-test or one-
422 way ANOVA was applied for normally distributed, homoscedastic data. Otherwise, the Wilcoxon
423 or Kruskal-Wallis test was used. All statistical tests were two-sided. P values from multi-
424 comparison tests were adjusted using the false discovery rate (FDR) method. Bar plots are
425 shown as mean ± SD. Box plots are shown as median and upper/lower quartiles, with whiskers
426 showing the 1.5× interquartile range. Each point in the dot plot represents a single cell or a
427 replicate. A density plot displaying the data distribution of each group is shown when applicable.

428 **Data availability**

429 HiC and CUT&RUN data will be uploaded to the NIH Sequence Read Archive (SRA) and made
430 publicly accessible upon the acceptance of the manuscript.

Acknowledgments

This work was supported by the Cancer Prevention and Research Institute of Texas (CPRIT, RR210034) and the Gilead's Research Scholars Program in Solid Tumors. J.Y.S. Lim. is supported by the CPRIT Training Grant (RP210041). Graphic illustrations were created using BioRender. We thank Dr. Pippa Cosper at the University of Wisconsin for her advice on this project.

Author contributions

Y. Xie and S. Wu conceptualized the research. Y. Xie, J.Y.S. Lim, and S. Wu developed the methodology and analyzed data. Y. Xie, J.Y.S. Lim, W. Liu, C. Gilbreath, and Y.J. Kim performed experiments. Y. Xie and S. Wu wrote the manuscript. Y.J. Kim and S. Wu supervised this research.

Declaration of interests

S. Wu is a member of the scientific advisory board of Dimension Genomics Inc. All other authors declare no competing interests.

446 # Figure legends

447 **Figure 1. Characterization of ecDNA interaction sites during mitosis. (A)** Illustration of
448 profiling ecDNA trans-interaction sites between G1 and M phases. **(B)** Representative *MYC* DNA
449 FISH image on MSTO211H cells at metaphase showing *MYC* ecDNAs (scale bar: 5 μm). **(C)**
450 HiC contact heatmap showing *MYC* ecDNA interactions between G1 and M phases. The *MYC*
451 ecDNA locus is highlighted. **(D)** HiC contact heatmap showing decreased *MYC* ecDNA trans-
452 interactions with chromosome 1 in the M phase compared to the G1 phase. **(E)** H3K27ac and
453 H3K4me3 coverage profiles between ecDNA trans-interaction sites and 1,000 randomly selected
454 10-kb genomic intervals. **(F)** H3K27ac and H3K4me3 read counts between ecDNA trans-
455 interaction sites and 1,000 randomly selected sites with 10-kb genomic intervals (two-sided
456 Wilcoxon test).

457 **Figure 2. Epigenetic regulators of ecDNA segregation. (A)** Illustration depicting the writers
458 of H3K27ac and H3K4me3 histone modifications. **(B)** Workflow showing the imaging approach
459 to study ecDNA interaction with chromosomes during metaphase. A 12-16 hours nocodazole
460 treatment was applied to enrich prophase and prometaphase cells after drug treatment or RNAi
461 transfection, followed by a washout to release the cell cycle into the metaphase and anaphase.
462 **(C)** H3K27ac CUT&RUN coverage profiles in DMSO, 5 μM A485, and 5 μM A485 +2 μM SAHA
463 treated MSTO211H cells. TSS: Transcription start site; TES: Transcription end site. **(D)**
464 Representative *MYC* ecDNA FISH on MSTO211H metaphase cells (scale bar: 5 μm). **(E)**
465 Increased number of detached *MYC* ecDNAs per MSTO211H metaphase cell after 5 μM A485
466 treatment and rescued by 2 μM SAHA treatment (Kruskal-Wallis test with post-hoc Dunn test,
467 two-sided). **(F)** Western blot showing decreased H3K27ac abundance in MSTO211H cells after
468 CBP/P300 RNAi knockdown. **(G)** Representative *MYC* ecDNA FISH on MSTO211H metaphase
469 cells after CBP/P300 knockdown (scale bar: 5 μm). **(H)** Elevated number of detached *MYC*
470 ecDNAs per MSTO211H metaphase cell after CBP/P300 knockdown (two-sided Wilcoxon test).

471 **Figure 3. Bromodomain proteins anchor ecDNAs to mitotic chromosomes. (A)** Illustration
472 of major bromodomain-containing proteins as the readers of H3K27ac histone modification. **(B)**
473 Representative *MYC* and *FGFR2* ecDNA FISH on 100 nM dBET6 treated SNU16 metaphase
474 cells (scale bar: 5 μm). **(C)** Increased number of detached *MYC* and *FGFR2* ecDNAs per SNU16
475 metaphase cells after dBET6 treatment (two-sided Wilcoxon test). **(D)** Western blot showing
476 dose-responding degradation of BRD4 or SMARCA4 after dBET6 or AU15330 treatment in
477 SNU16 cells. **(E)** Representative *MYC* ecDNA FISH on 200 nM dBET6 or 1000 nM AU15330
478 treated MSTO211H metaphase cells (scale bar: 5 μm). **(F)** The number of detached *MYC*
479 ecDNAs per MSTO211H metaphase cell after dBET6 or AU15330 treatment (Kruskal-Wallis test
480 with post-hoc Dunn test). **(G)** Representative *MYC* ecDNA FISH on 200 nM dBET6 and 1000
481 nM AU15330 treated MSTO211H metaphase cells (scale bar: 5 μm). **(H)** Increased number of
482 detached *MYC* ecDNAs per MSTO211H metaphase cell after dBET6+AU15330 treatment (two-
483 sided Wilcoxon test).

484 **Figure 4. The kinase module of the Mediator complex regulates ecDNA segregation. (A)**
485 Illustration depicting the Mediator complex components. **(B)** *CDK8* or Cyclin C RNAi knockdown
486 efficiency measured by mRNA qPCR in MSTO211H cells (two-sided Student's t-test). **(C)**
487 Representative *MYC* ecDNA FISH on MSTO211H metaphase cells after *CDK8* knockdown
488 (scale bar: 5 μm). **(D)** The number of detached *MYC* ecDNAs per MSTO211H metaphase cell
489 after *CDK8* RNAi knockdown (two-sided Wilcoxon test). **(E)** Representative *MYC* ecDNA FISH
490 on MSTO211H metaphase cells after Cyclin C knockdown (scale bar: 5 μm). **(F)** The number of
491 detached *MYC* ecDNAs per MSTO211H metaphase cell after Cyclin C RNAi knockdown (two-
492 sided Wilcoxon test). **(G)** *MED13* RNAi knockdown efficiency assessed by qPCR in MSTO211H
493 cells (two-sided Student's t-test). **(H)** Representative *MYC* ecDNA FISH images showing the
494 rescue effect of *MED13* knockdown in ecDNA attachment to mitotic chromosomes (scale bar: 5
495 μm). **(I)** Quantification of the number of detached *MYC* ecDNAs per MSTO211H metaphase cell
496 after *CDK8* and *MED13* RNAi knockdown (Kruskal-Wallis test with post-hoc Dunn test).

497 **Figure 5. Mitotic transcription is required for ecDNA segregation. (A)** Illustration of
498 transcription or translation inhibitors in this study. **(B)** Workflow showing the imaging approach
499 to study ecDNA attachment with mitotic chromosomes during metaphase. A 12-hr nocodazole
500 treatment was first applied to enrich prophase and prometaphase cells. Two or six hours before
501 the nocodazole treatment endpoint, a transcription or translation inhibitor was added to cell
502 culture, before washing out to release cells into metaphase and anaphase for fixation and
503 imaging. **(C)** Representative *MYC* ecDNA FISH on MSTO211H metaphase cells after 2 μM
504 actinomycin D or 2 μM triptolide treatment (scale bar: 5 μm). **(D)** Representative *MYC* ecDNA
505 FISH on MSTO211H metaphase cells after 100 μg mL^{-1} α-amanitin treatment (scale bar: 5 μm).
506 **(E)** The number of detached *MYC* ecDNAs per MSTO211H metaphase cell after actinomycin D,
507 triptolide (Kruskal-Wallis test with post-hoc Dunn test), or α-amanitin treatment (two-sided
508 Wilcoxon test). **(F)** Proposed molecular machinery anchoring ecDNAs to mitotic chromosomes
509 for segregation**.**

510 **Figure 6. The consequence of mis-segregated ecDNAs. (A)** Live-cell imaging with
511 COLO320DM TetO-MYC TetR-mNeonGreen cell line under the treatment with 1000 nM dBET6
512 (scale bar: 5 μm. White arrow: Detached ecDNA. Yellow arrow: Micronuclei-like morphology).
513 **(B)** Workflow showing the long-term dBET6 or A485 treatment for functional assessments.
514 ecDNA copy number was quantified by qPCR every week after treatment. dBET6 was washed
515 out at least 24 hours before cell viability assessment by CCK8 assays. **(C)** qPCR results showing
516 continuously decreased *MYC* ecDNA copy number in MSTO211H cells after 1-3 weeks of A485
517 treatment (one-way ANNOVA with post-hoc Dunnett test). **(D)** Representative *DHFR* ecDNA
518 FISH on HeLa-ecDHFR metaphase cells after 50 nM dBET6 treatment (scale bar: 5 μm). **(E)**
519 Increased number of detached *DHFR* ecDNAs per HeLa-ecDHFR metaphase cell after dBET6
520 treatment (two-sided Wilcoxon test). **(F)** qPCR results for *DHFR* ecDNA copy number in HeLa-
521 ecDHFR cells after 1-4 weeks of dBET6 treatment (two-sided Student's t-test). **(G)** Methotrexate-

522 cell viability dose-response curves for HeLa-ecDHFR cells comparing cells pre-treated with
523 DMSO or dBET6 for 4 weeks.

524 # Supplementary figure legends

525 **Figure S1. HiC analysis to identify the epigenetic features of ecDNA trans-interaction sites**
526 **during mitosis. (A)** Abundant H3K27ac and H3K4me3 are present on ecDNAs at metaphase,
527 determined by immunofluorescence. Arrows indicate ecDNAs (scale bar: 5 μm). **(B)** Workflow of
528 integrative analysis of HiC and CUT&RUN data. Two HiC replicates from G1 and M phases
529 sorted cell fraction were processed by the HiC-Pro pipeline to obtain contact maps. After the
530 reproducibility check, replicates from the same cell cycle fraction were merged for trans-
531 interaction analysis. Top interaction loci were extracted for subsequent CUT&RUN coverage
532 analysis. **(C)** WGS track of MSTO211H cells showing the *MYC* ecDNA locus. **(D)** Number of
533 valid pairs of each HiC library. **(E)** Stratum-adjusted correlation coefficient matrix among HiC
534 libraries. **(F)** Density distribution of ecDNA trans-interaction contact counts in G1 and M phases.
535 The top 0.1% ecDNA-derived trans-interactions were defined as significant interaction sites. **(G)**
536 Representative H3K27ac and H3K4me3 coverage tracks of the ecDNA interaction sites.

537 **Figure S2. Histone modifications facilitating ecDNA segregation. (A)** Western blot showing
538 a dose-response of H3K27ac downregulation after A485 treatment in SNU16 cells. **(B)**
539 Representative *MYC* and *FGFR2* ecDNA FISH on 10 μM A485 treated SNU16 metaphase cells
540 (scale bar: 5 μm). **(C)** The number of detached *MYC* and *FGFR2* ecDNA per SNU16 metaphase
541 cell after A485 treatment (two-sided Wilcoxon test). **(D)** Dose-responding H3K27ac
542 downregulation after A485 treatment in COLO320DM cells measured with Western blot. **(E)**
543 Representative *MYC* ecDNA FISH on A485 treated COLO320DM metaphase cells (scale bar: 5
544 μm). **(F)** Elevated number of detached *MYC* ecDNAs per COLO320DM metaphase cell after
545 A485 treatment (two-sided Wilcoxon test). **(G)** Western blot for H3K27ac in MSTO211H cells
546 after A485 and SAHA treatment. **(H)** Representative CUT&RUN coverage tracks for H3K27ac
547 after 5 μM A485 and 2 μM SAHA treatment in MSTO211H cells. **(I)** Western blot showing
548 decreased H3K4me3 after *DPY30* and *RBBP5* RNAi knockdown in SNU16 cells. **(J)**
549 Representative *MYC* and *FGFR2* ecDNA FISH on SNU16 metaphase cells after *DPY30* and
550 *RBBP5* knockdown (scale bar: 5 μm). **(K)** The number of detached *MYC* and *FGFR2* ecDNA per
551 SNU16 metaphase cell after *DPY30* and *RBBP5* RNAi knockdown (two-sided Wilcoxon test).

552 **Figure S3. BET proteins in ecDNA segregation. (A)** Heatmap for the mRNA expression level
553 of all human bromodomain-containing proteins in ecDNA cancer cell lines. Data were obtained
554 from public RNAseq. TPM: transcripts per million. **(B)** Western blot for BRD2, BRD3, and BRD4
555 in SNU16 cells after dBET6 treatment for 24 hours. **(C)** Western blot showing BRD4 degradation
556 after dBET6 treatment for 24 hours in COLO320DM cells. **(D)** Representative *MYC* ecDNA FISH
557 on 1000 nM dBET6 treated COLO320DM metaphase cells (scale bar: 5 μm). **(E)** The number of
558 detached *MYC* ecDNA per COLO320DM metaphase cell after dBET6 treatment (two-sided
559 Wilcoxon test). **(F)** RNAi knockdown efficiency of *BRD2*, *BRD3*, and *BRD4* quantified using
560 qPCR (two-sided Student's t-test). **(G)** Representative *MYC* and *FGFR2* ecDNA FISH in SNU16
561 metaphase cells after *BRD2*, *BRD3*, or *BRD4* RNAi knockdown (scale bar: 5 μm). **(H)** The

number of detached *MYC* and *FGFR2* ecDNAs per SNU16 metaphase cell after *BRD2*, *BRD3*, or *BRD4* RNAi knockdown (Kruskal-Wallis test with post-hoc Dunn test). **(I)** Western blot for BRD4 and HA tag in COLO320DM-BRD4::FKBP12^{F36V} cells after dTAGv1 treatment. **(J)** Representative *MYC* ecDNA FISH on COLO320DM-BRD4::FKBP12^{F36V} metaphase cells after 500 nM dTAGv1 treatment (scale bar: 5 μm). **(K)** The number of detached *MYC* ecDNA per COLO320DM-BRD4::FKBP12^{F36V} metaphase cell after dTAGv1 treatment (two-sided Wilcoxon test).

Figure S4. The kinase module of the Mediator complex regulates ecDNA segregation in SNU16 cells. (A) qPCR results for Cyclin C and *CDK8* mRNA level in SNU16 cells after corresponding RNAi knockdown (two-sided Student's t-test). **(B)** Representative *MYC* and *FGFR2* ecDNA FISH in SNU16 metaphase cells after Cyclin C or *CDK8* RNAi knockdown (scale bar: 5 μm). **(C)** The number of detached *MYC* and *FGFR2* ecDNA per SNU16 metaphase cell after Cyclin C or *CDK8* RNAi knockdown (Kruskal-Wallis test with post-hoc Dunn test).

Figure S5. Mitotic transcription and translation dependency for ecDNA segregation. (A) Western blot for total and phospho-RPB1 Ser2/5 in MSTO211H cells after transcription inhibitors treatment. **(B)** qPCR results for *MYC* mRNA level in MSTO211H cells after transcription inhibitors treatment. The long half-life *RPL13A* transcript was used for normalization (one-way ANNOVA with post-hoc Dunnett test). **(C)** Western blot for BRD4, SMARCA4, and CDK8 in MSTO211H cells after transcription inhibitors treatment, showing limited impact on their protein levels after short-term inhibition of transcription. **(D)** Representative images for O-propargyl-puromycin signal, which represents nascent protein synthesis, in MSTO211H cells after 5 μg mL^{-1} cycloheximide treatment (scale bar: 5 μm). **(E)** Representative *MYC* ecDNA FISH in MSTO211H metaphase cells after 2 μM triptolide or 5μg mL^{-1} cycloheximide treatment (scale bar: 5 μm). The 2-hour triptolide treatment served as the positive control (scale bar: 5 μm). **(F)** The number of detached *MYC* ecDNA per MSTO211H metaphase cell after triptolide or cycloheximide treatment (Kruskal-Wallis test with post-hoc Dunn test).

Figure S6. Mis-segregated ecDNAs reduces oncogenicity. (A) Representative *MYC* and *FGFR2* ecDNA FISH in SNU16 interphase cells. Cells were treated with 10 μM A485 with a nocodazole arrest and were subsequently released to the next cell cycle (scale bar: 5 μm). **(B)** Cytosolic *MYC* and *FGFR2* ecDNAs per SNU16 interphase cell as measured by square pixel of FISH signal outside of the main nucleus (two-sided Wilcoxon test). **(C)** Western blot for MYC in MSTO211H cells after 2 weeks of A485 treatment. **(D)** Western blot for BRD4 in HeLa-ecDHFR cells after dBET6 treatment.

References

1. Chen, X., Agustinus, A.S., Li, J., DiBona, M., and Bakhoum, S.F. (2025). Chromosomal instability as a driver of cancer progression. Nat. Rev. Genet. *26*, 31–46.

2. Verdaasdonk, J.S., and Bloom, K. (2011). Centromeres: unique chromatin structures that drive chromosome segregation. Nat. Rev. Mol. Cell Biol. *12*, 320–332.

3. Valdez, V.A., Neahring, L., Petry, S., and Dumont, S. (2023). Mechanisms underlying spindle assembly and robustness. Nat. Rev. Mol. Cell Biol. *24*, 523–542.

4. Yi, E., Chamorro González, R., Henssen, A.G., and Verhaak, R.G.W. (2022). Extrachromosomal DNA amplifications in cancer. Nat. Rev. Genet. *23*, 760–771.

5. Kim, H., Nguyen, N.-P., Turner, K., Wu, S., Gujar, A.D., Luebeck, J., Liu, J., Deshpande, V., Rajkumar, U., Namburi, S., et al. (2020). Extrachromosomal DNA is associated with oncogene amplification and poor outcome across multiple cancers. Nat. Genet. *52*, 891–897.

6. Turner, K.M., Deshpande, V., Beyter, D., Koga, T., Rusert, J., Lee, C., Li, B., Arden, K., Ren, B., Nathanson, D.A., et al. (2017). Extrachromosomal oncogene amplification drives tumour evolution and genetic heterogeneity. Nature *543*, 122–125.

7. Kim, H., Kim, S., Wade, T., Yeo, E., Lipsa, A., Golebiewska, A., Johnson, K.C., An, S., Ko, J., Nam, Y., et al. (2024). Mapping extrachromosomal DNA amplifications during cancer progression. Nat. Genet. *56*, 2447–2454.

8. Hung, K.L., Luebeck, J., Dehkordi, S.R., Colón, C.I., Li, R., Wong, I.T.-L., Coruh, C., Dharanipragada, P., Lomeli, S.H., Weiser, N.E., et al. (2022). Targeted profiling of human extrachromosomal DNA by CRISPR-CATCH. Nat. Genet. *54*, 1746–1754.

9. Bailey, C., Pich, O., Thol, K., Watkins, T.B.K., Luebeck, J., Rowan, A., Stavrou, G., Weiser, N.E., Dameracharla, B., Bentham, R., et al. (2024). Origins and impact of extrachromosomal DNA. Nature *635*, 193–200.

10. Wu, S., Turner, K.M., Nguyen, N., Raviram, R., Erb, M., Santini, J., Luebeck, J., Rajkumar, U., Diao, Y., Li, B., et al. (2019). Circular ecDNA promotes accessible chromatin and high oncogene expression. Nature *575*, 699–703.

11. Rodríguez-Beltrán, J., DelaFuente, J., León-Sampedro, R., MacLean, R.C., and San Millán, Á. (2021). Beyond horizontal gene transfer: the role of plasmids in bacterial evolution. Nat. Rev. Microbiol. *19*, 347–359.

12. Wu, S., Bafna, V., Chang, H.Y., and Mischel, P.S. (2022). Extrachromosomal DNA: An Emerging Hallmark in Human Cancer. Annu. Rev. Pathol. *17*, 367–386.

13. Lange, J.T., Rose, J.C., Chen, C.Y., Pichugin, Y., Xie, L., Tang, J., Hung, K.L., Yost, K.E., Shi, Q., Erb, M.L., et al. (2022). The evolutionary dynamics of extrachromosomal DNA in human cancers. Nat. Genet. *54*, 1527–1533.

14. Noer, J.B., Hørsdal, O.K., Xiang, X., Luo, Y., and Regenberg, B. (2022). Extrachromosomal circular DNA in cancer: history, current knowledge, and methods. Trends Genet. *38*, 766–781.

15. Pal Choudhuri, S., Girard, L., Lim, J.Y.S., Wise, J.F., Freitas, B., Yang, D., Wong, E., Hamilton, S., Chien, V.D., Kim, Y.J., et al. (2024). Acquired Cross-Resistance in Small Cell Lung Cancer due to Extrachromosomal DNA Amplification of MYC Paralogs. Cancer Discov. *14*, 804–827.

16. deCarvalho, A.C., Kim, H., Poisson, L.M., Winn, M.E., Mueller, C., Cherba, D., Koeman, J., Seth, S., Protopopov, A., Felicella, M., et al. (2018). Discordant inheritance of chromosomal and extrachromosomal DNA elements contributes to dynamic disease evolution in glioblastoma. Nat. Genet. *50*, 708–717.

17. Chapman, O.S., Luebeck, J., Sridhar, S., Wong, I.T.-L., Dixit, D., Wang, S., Prasad, G., Rajkumar, U., Pagadala, M.S., Larson, J.D., et al. (2023). Circular extrachromosomal DNA promotes tumor heterogeneity in high-risk medulloblastoma. Nat. Genet. *55*, 2189–2199.

18. Hung, K.L., Jones, M.G., Wong, I.T.-L., Curtis, E.J., Lange, J.T., He, B.J., Luebeck, J., Schmargon, R., Scanu, E., Brückner, L., et al. (2024). Coordinated inheritance of extrachromosomal DNAs in cancer cells. Nature *635*, 201–209.

19. Levan, A., and Levan, G. (1978). Have double minutes functioning centromeres? Hereditas *88*, 81–92.

20. Kanda, T., Otter, M., and Wahl, G.M. (2001). Mitotic segregation of viral and cellular acentric extrachromosomal molecules by chromosome tethering. J. Cell Sci. *114*, 49–58.

21. Yi, E., Gujar, A.D., Guthrie, M., Kim, H., Zhao, D., Johnson, K.C., Amin, S.B., Costa, M.L., Yu, Q., Das, S., et al. (2022). Live-cell imaging shows uneven segregation of extrachromosomal DNA elements and transcriptionally active extrachromosomal DNA hubs in cancer. Cancer Discov. *12*, 468–483.

22. Zhu, Y., Gujar, A.D., Wong, C.-H., Tjong, H., Ngan, C.Y., Gong, L., Chen, Y.-A., Kim, H., Liu, J., Li, M., et al. (2021). Oncogenic extrachromosomal DNA functions as mobile enhancers to globally amplify chromosomal transcription. Cancer Cell *39*, 694-707.e7.

23. Zhang, H., Emerson, D.J., Gilgenast, T.G., Titus, K.R., Lan, Y., Huang, P., Zhang, D., Wang, H., Keller, C.A., Giardine, B., et al. (2019). Chromatin structure dynamics during the mitosis-to-G1 phase transition. Nature *576*, 158–162.

24. Naumova, N., Imakaev, M., Fudenberg, G., Zhan, Y., Lajoie, B.R., Mirny, L.A., and Dekker, J. (2013). Organization of the mitotic chromosome. Science *342*, 948–953.

25. Nagano, T., Lubling, Y., Várnai, C., Dudley, C., Leung, W., Baran, Y., Mendelson Cohen, N., Wingett, S., Fraser, P., and Tanay, A. (2017). Cell-cycle dynamics of chromosomal organization at single-cell resolution. Nature *547*, 61–67.

26. Millán-Zambrano, G., Burton, A., Bannister, A.J., and Schneider, R. (2022). Histone post-translational modifications - cause and consequence of genome function. Nat. Rev. Genet. *23*, 563–580.

27. Lasko, L.M., Jakob, C.G., Edalji, R.P., Qiu, W., Montgomery, D., Digiammarino, E.L., Hansen, T.M., Risi, R.M., Frey, R., Manaves, V., et al. (2017). Discovery of a selective catalytic p300/CBP inhibitor that targets lineage-specific tumours. Nature *550*, 128–132.

28. Slaughter, M.J., Shanle, E.K., Khan, A., Chua, K.F., Hong, T., Boxer, L.D., Allis, C.D., Josefowicz, S.Z., Garcia, B.A., Rothbart, S.B., et al. (2021). HDAC inhibition results in widespread alteration of the histone acetylation landscape and BRD4 targeting to gene bodies. Cell Rep. *34*, 108638.

29. Shvedunova, M., and Akhtar, A. (2022). Modulation of cellular processes by histone and non-histone protein acetylation. Nat. Rev. Mol. Cell Biol. *23*, 329–349.

30. Wang, H., and Helin, K. (2024). Roles of H3K4 methylation in biology and disease. Trends Cell Biol. *0*. https://doi.org/10.1016/j.tcb.2024.06.001.

31. Cenik, B.K., and Shilatifard, A. (2021). COMPASS and SWI/SNF complexes in development and disease. Nat. Rev. Genet. *22*, 38–58.

32. Wang, H., Fan, Z., Shliaha, P.V., Miele, M., Hendrickson, R.C., Jiang, X., and Helin, K. (2023). H3K4me3 regulates RNA polymerase II promoter-proximal pause-release. Nature *615*, 339–348.

33. Fujisawa, T., and Filippakopoulos, P. (2017). Functions of bromodomain-containing proteins and their roles in homeostasis and cancer. Nat. Rev. Mol. Cell Biol. *18*, 246–262.

34. Tsherniak, A., Vazquez, F., Montgomery, P.G., Weir, B.A., Kryukov, G., Cowley, G.S., Gill, S., Harrington, W.F., Pantel, S., Krill-Burger, J.M., et al. (2017). Defining a cancer dependency map. Cell *170*, 564-576.e16.

35. Winter, G.E., Mayer, A., Buckley, D.L., Erb, M.A., Roderick, J.E., Vittori, S., Reyes, J.M., di Iulio, J., Souza, A., Ott, C.J., et al. (2017). BET bromodomain proteins function as master transcription elongation factors independent of CDK9 recruitment. Mol. Cell *67*, 5-18.e19.

36. Hung, K.L., Yost, K.E., Xie, L., Shi, Q., Helmsauer, K., Luebeck, J., Schöpflin, R., Lange, J.T., Chamorro González, R., Weiser, N.E., et al. (2021). ecDNA hubs drive cooperative intermolecular oncogene expression. Nature *600*, 731–736.

37. Xiao, L., Parolia, A., Qiao, Y., Bawa, P., Eyunni, S., Mannan, R., Carson, S.E., Chang, Y., Wang, X., Zhang, Y., et al. (2022). Targeting SWI/SNF ATPases in enhancer-addicted prostate cancer. Nature *601*, 434–439.

701 38. Jeronimo, C., and Robert, F. (2017). The Mediator complex: At the nexus of RNA
702 polymerase II transcription. Trends Cell Biol. *27*, 765–783.

703 39. Richter, W.F., Nayak, S., Iwasa, J., and Taatjes, D.J. (2022). The Mediator complex as a
704 master regulator of transcription by RNA polymerase II. Nat. Rev. Mol. Cell Biol. *23*, 732–
705 749.

706 40. Allen, B.L., and Taatjes, D.J. (2015). The Mediator complex: a central integrator of
707 transcription. Nat. Rev. Mol. Cell Biol. *16*, 155–166.

708 41. Clark, A.D., Oldenbroek, M., and Boyer, T.G. (2015). Mediator kinase module and human
709 tumorigenesis. Crit. Rev. Biochem. Mol. Biol. *50*, 393–426.

710 42. Davis, M.A., Larimore, E.A., Fissel, B.M., Swanger, J., Taatjes, D.J., and Clurman, B.E.
711 (2013). The SCF-Fbw7 ubiquitin ligase degrades MED13 and MED13L and regulates CDK8
712 module association with Mediator. Genes Dev. *27*, 151–156.

713 43. Osman, S., Mohammad, E., Lidschreiber, M., Stuetzer, A., Bazsó, F.L., Maier, K.C., Urlaub,
714 H., and Cramer, P. (2021). The Cdk8 kinase module regulates interaction of the mediator
715 complex with RNA polymerase II. J. Biol. Chem. *296*, 100734.

716 44. Dani, C., Blanchard, J.M., Piechaczyk, M., El Sabouty, S., Marty, L., and Jeanteur, P. (1984).
717 Extreme instability of myc mRNA in normal and transformed human cells. Proc. Natl. Acad.
718 Sci. U. S. A. *81*, 7046–7050.

719 45. Shoshani, O., Brunner, S.F., Yaeger, R., Ly, P., Nechemia-Arbely, Y., Kim, D.H., Fang, R.,
720 Castillon, G.A., Yu, M., Li, J.S.Z., et al. (2021). Chromothripsis drives the evolution of gene
721 amplification in cancer. Nature *591*, 137–141.

722 46. Kaufman, R.J., Brown, P.C., and Schimke, R.T. (1979). Amplified dihydrofolate reductase
723 genes in unstably methotrexate-resistant cells are associated with double minute
724 chromosomes. Proc. Natl. Acad. Sci. U. S. A. *76*, 5669–5673.

725 47. Teves, S.S., An, L., Bhargava-Shah, A., Xie, L., Darzacq, X., and Tjian, R. (2018). A stable
726 mode of bookmarking by TBP recruits RNA polymerase II to mitotic chromosomes. Elife *7*.
727 https://doi.org/10.7554/eLife.35621.

728 48. White, J., Derheimer, F.A., Jensen-Pergakes, K., O'Connell, S., Sharma, S., Spiegel, N.,
729 and Paul, T.A. (2024). Histone lysine acetyltransferase inhibitors: an emerging class of
730 drugs for cancer therapy. Trends Pharmacol. Sci. *45*, 243–254.

731 49. Yu, X., Zhao, H., Wang, R., Chen, Y., Ouyang, X., Li, W., Sun, Y., and Peng, A. (2024).
732 Cancer epigenetics: from laboratory studies and clinical trials to precision medicine. Cell
733 Death Discov. *10*, 28.

734 50. Dai, W., Qiao, X., Fang, Y., Guo, R., Bai, P., Liu, S., Li, T., Jiang, Y., Wei, S., Na, Z., et al.
735 (2024). Epigenetics-targeted drugs: current paradigms and future challenges. Signal
736 Transduct. Target. Ther. *9*, 332.

737 51. Dziadziunszko, R., Garralda, E., Angelosanto, N., Rzymski, T., Dudziak, R., Brzózka, K.,
738 Littlewood, P., Nogai, H., Glasmacher, A.G., and Lugowska, I. (2022). Phase I/II trial of
739 RVU120 (SEL120), a CDK8/CDK19 inhibitor in patients with relapsed/refractory metastatic
740 or advanced solid tumors. J. Clin. Oncol. *40*, e15091–e15091.

741 52. Ablasser, A., and Chen, Z.J. (2019). cGAS in action: Expanding roles in immunity and
742 inflammation. Science *363*, eaat8657.

743 53. Chen, Q., Sun, L., and Chen, Z.J. (2016). Regulation and function of the cGAS-STING
744 pathway of cytosolic DNA sensing. Nat. Immunol. *17*, 1142–1149.

745 54. Kang, H., Shokhirev, M.N., Xu, Z., Chandran, S., Dixon, J.R., and Hetzer, M.W. (2020).
746 Dynamic regulation of histone modifications and long-range chromosomal interactions
747 during postmitotic transcriptional reactivation. Genes Dev. *34*, 913–930.

748 55. Javasky, E., Shamir, I., Gandhi, S., Egri, S., Sandler, O., Rothbart, S.B., Kaplan, N., Jaffe,
749 J.D., Goren, A., and Simon, I. (2018). Study of mitotic chromatin supports a model of
750 bookmarking by histone modifications and reveals nucleosome deposition patterns.
751 Genome Res. *28*, 1455–1466.

752 56. Liu, Y., Pelham-Webb, B., Di Giammartino, D.C., Li, J., Kim, D., Kita, K., Saiz, N., Garg, V.,
753 Doane, A., Giannakakou, P., et al. (2017). Widespread mitotic bookmarking by histone
754 marks and transcription factors in pluripotent stem cells. Cell Rep. *19*, 1283–1293.

755 57. Bellec, M., Dufourt, J., Hunt, G., Lenden-Hasse, H., Trullo, A., Zine El Aabidine, A.,
756 Lamarque, M., Gaskill, M.M., Faure-Gautron, H., Mannervik, M., et al. (2022). The control
757 of transcriptional memory by stable mitotic bookmarking. Nat. Commun. *13*, 1176.

758 58. Yu, Q., Liu, X., Fang, J., Wu, H., Guo, C., Zhang, W., Liu, N., Jiang, C., Sha, Q., Yuan, X.,
759 et al. (2023). Dynamics and regulation of mitotic chromatin accessibility bookmarking at
760 single-cell resolution. Sci. Adv. *9*, eadd2175.

761 59. Meers, M.P., Bryson, T.D., Henikoff, J.G., and Henikoff, S. (2019). Improved CUT&RUN
762 chromatin profiling tools. Elife *8*. https://doi.org/10.7554/eLife.46314.

Figure 1

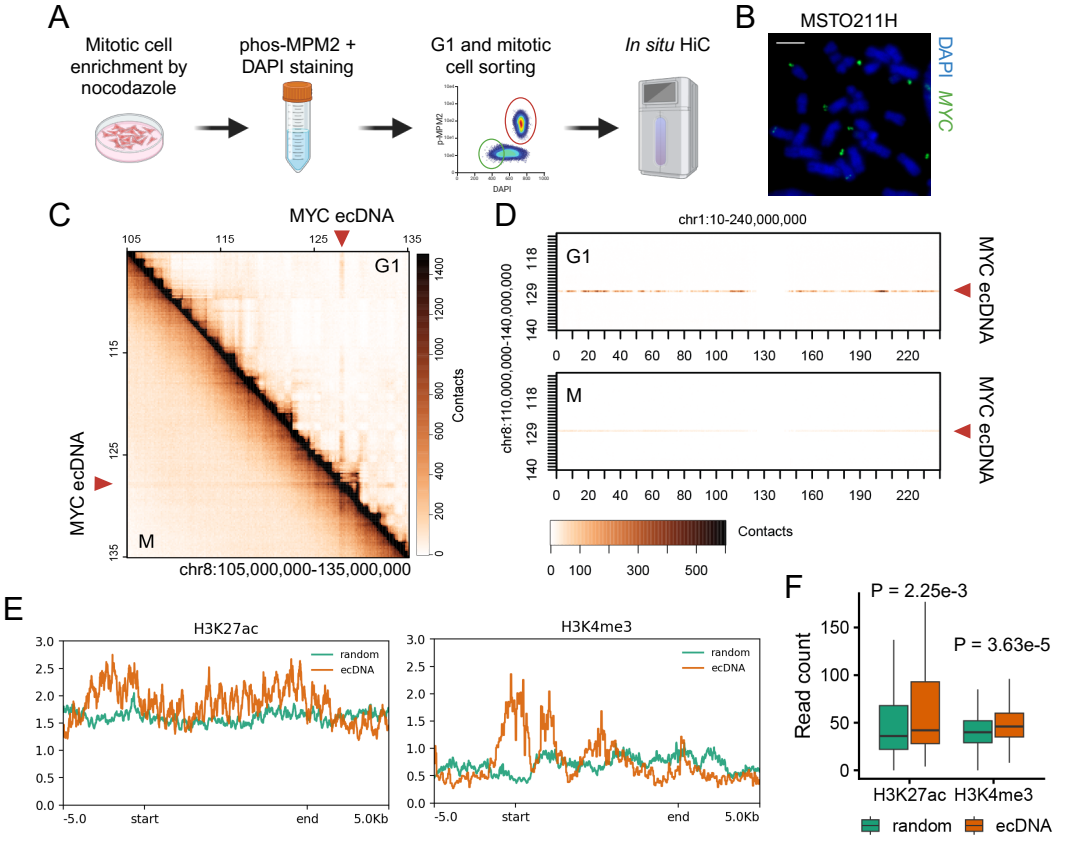
A
Mitotic cell enrichment by nocodazole
phos-MPM2 + DAPI staining
G1 and mitotic cell sorting
In situ HiC
B
MSTO211H
DAPI
MYC
C
MYC ecDNA
G1
M
MYC ecDNA
chr8:105,000,000-135,000,000
Contacts
D
chr1:10-240,000,000
G1
chr8:110,000,000-140,000,000
M
MYC ecDNA
Contacts
E
H3K27ac
H3K4me3
random
ecDNA
start
end
5.0Kb
F
P = 2.25e-3
P = 3.63e-5
Read count
H3K27ac
H3K4me3
random
ecDNA

Figure 2

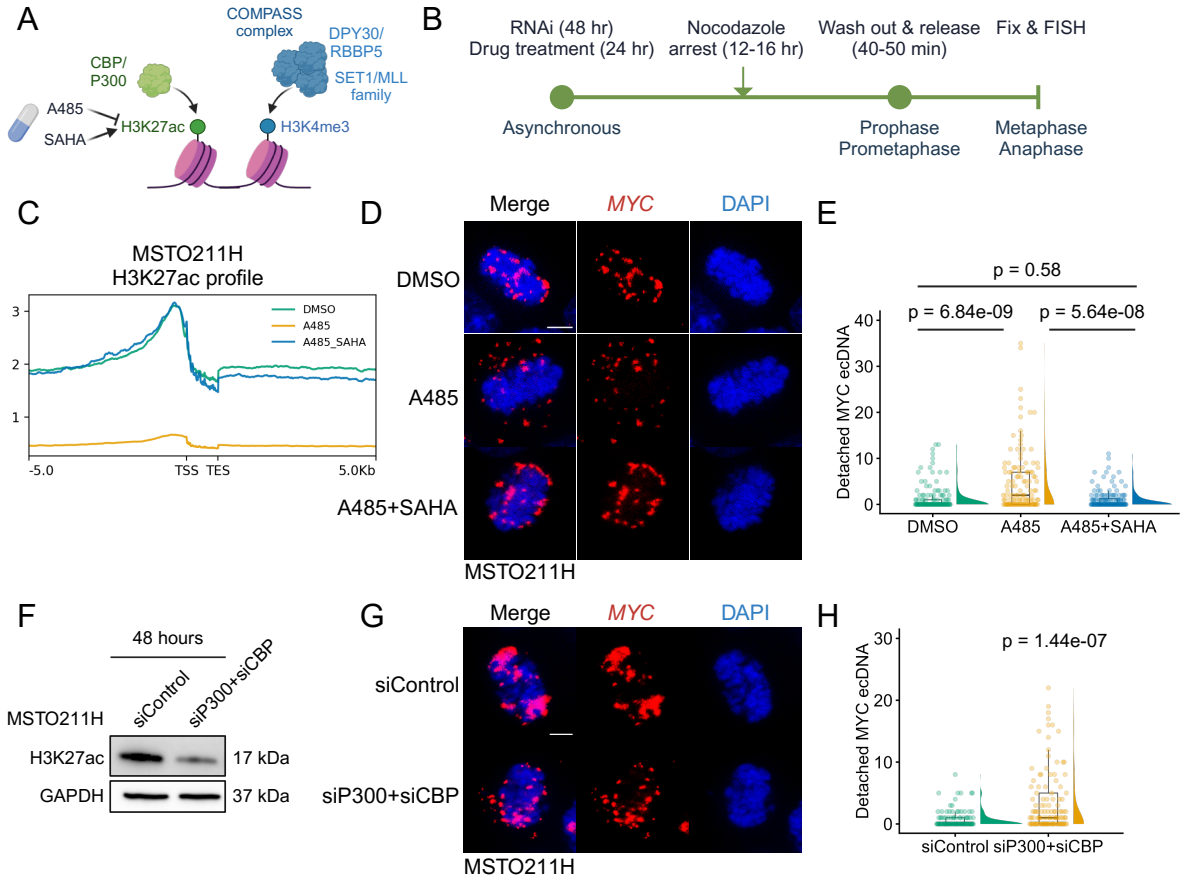
A
COMPASS complex
DPY30/ RBBP5
SET1/MLL family
CBP/ P300
A485
SAHA
H3K27ac
H3K4me3
B
RNAi (48 hr)
Drug treatment (24 hr)
Nocodazole arrest (12-16 hr)
Wash out & release (40-50 min)
Fix & FISH
Asynchronous
Prophase Prometaphase
Metaphase Anaphase
C
MSTO211H
H3K27ac profile
DMSO
A485
A485_SAHA
-5.0
TSS TES
5.0Kb
D
Merge
MYC
DAPI
DMSO
A485
A485+SAHA
MSTO211H
E
p = 0.58
p = 6.84e-09
p = 5.64e-08
Detached MYC ecDNA
DMSO
A485
A485+SAHA
F
48 hours
siControl
siP300+siCBP
MSTO211H
H3K27ac
GAPDH
17 kDa
37 kDa
G
Merge
MYC
DAPI
siControl
siP300+siCBP
MSTO211H
H
p = 1.44e-07
Detached MYC ecDNA
siControl
siP300+siCBP

Figure 3

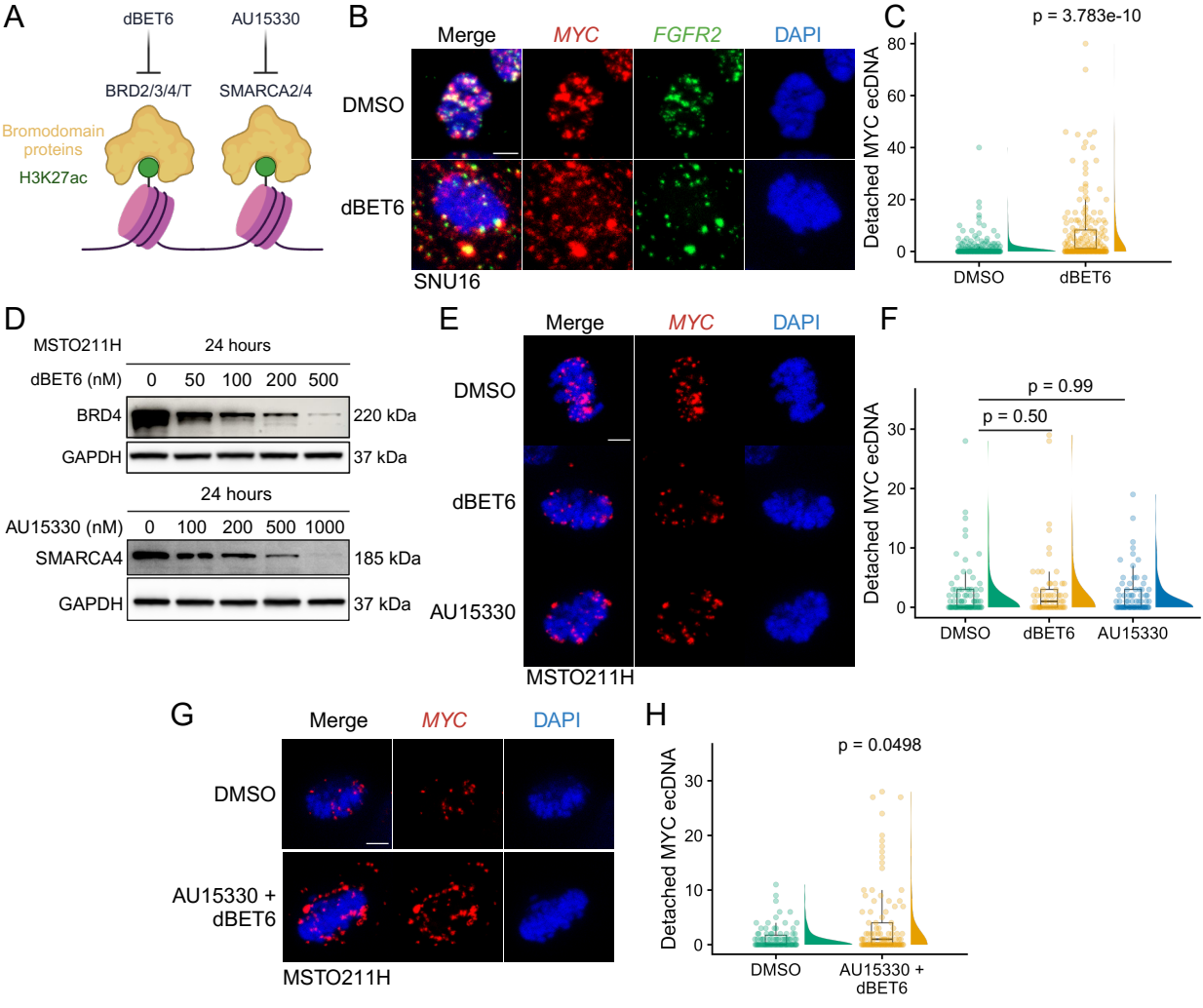
A
dBET6
AU15330
BRD2/3/4/T
SMARCA2/4
Bromodomain proteins
H3K27ac
B
Merge
MYC
FGFR2
DAPI
DMSO
dBET6
SNU16
C
p = 3.783e-10
Detached MYC ecDNA
80
60
40
20
0
DMSO
dBET6
D
MSTO211H
24 hours
dBET6 (nM)
0
50
100
200
500
BRD4
220 kDa
GAPDH
37 kDa
24 hours
AU15330 (nM)
0
100
200
500
1000
SMARCA4
185 kDa
GAPDH
37 kDa
E
Merge
MYC
DAPI
DMSO
dBET6
AU15330
MSTO211H
F
p = 0.99
p = 0.50
Detached MYC ecDNA
30
20
10
0
DMSO
dBET6
AU15330
G
Merge
MYC
DAPI
DMSO
AU15330 + dBET6
MSTO211H
H
p = 0.0498
Detached MYC ecDNA
30
20
10
0
DMSO
AU15330 + dBET6

Figure 4

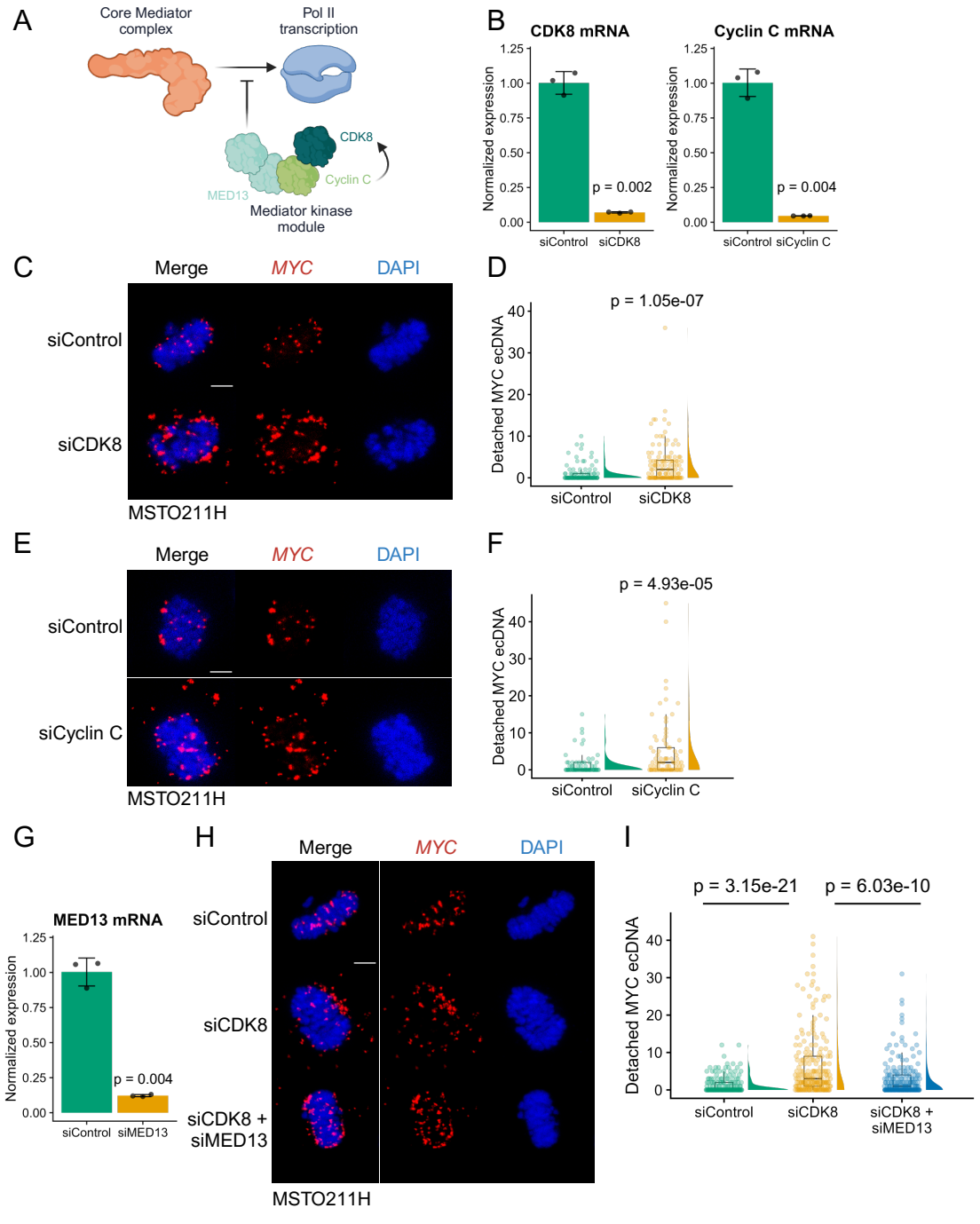
A
Core Mediator complex
Pol II transcription
CDK8
Cyclin C
MED13
Mediator kinase module
B
CDK8 mRNA
Cyclin C mRNA
Normalized expression
p = 0.002
p = 0.004
siControl
siCDK8
siCyclin C
C
Merge
MYC
DAPI
siControl
siCDK8
MSTO211H
D
p = 1.05e-07
Detached MYC ecDNA
siControl
siCDK8
E
Merge
MYC
DAPI
siControl
siCyclin C
MSTO211H
F
p = 4.93e-05
Detached MYC ecDNA
siControl
siCyclin C
G
MED13 mRNA
Normalized expression
p = 0.004
siControl
siMED13
H
Merge
MYC
DAPI
siControl
siCDK8
siCDK8 + siMED13
MSTO211H
I
p = 3.15e-21
p = 6.03e-10
Detached MYC ecDNA
siControl
siCDK8
siCDK8 + siMED13

Figure 5

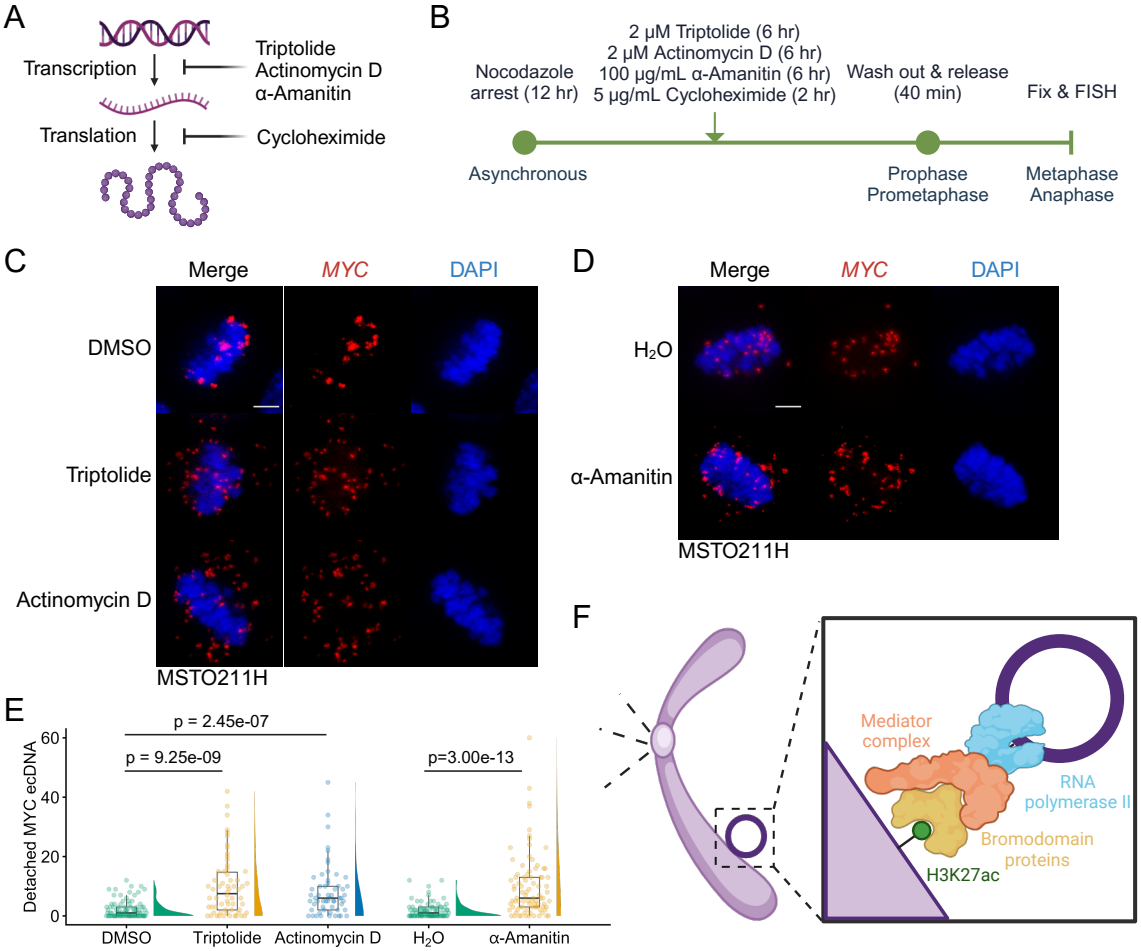
A
Transcription
Translation
Triptolide
Actinomycin D
α-Amanitin
Cycloheximide
B
Nocodazole arrest (12 hr)
2 μM Triptolide (6 hr)
2 μM Actinomycin D (6 hr)
100 μg/mL α-Amanitin (6 hr)
5 μg/mL Cycloheximide (2 hr)
Wash out & release (40 min)
Fix & FISH
Asynchronous
Prophase Prometaphase
Metaphase Anaphase
C
Merge
MYC
DAPI
DMSO
Triptolide
Actinomycin D
MSTO211H
D
Merge
MYC
DAPI
H2O
α-Amanitin
MSTO211H
E
p = 2.45e-07
p = 9.25e-09
p=3.00e-13
Detached MYC ecDNA
60
40
20
0
DMSO
Triptolide
Actinomycin D
H2O
α-Amanitin
F
Mediator complex
RNA polymerase II
Bromodomain proteins
H3K27ac

Figure 6

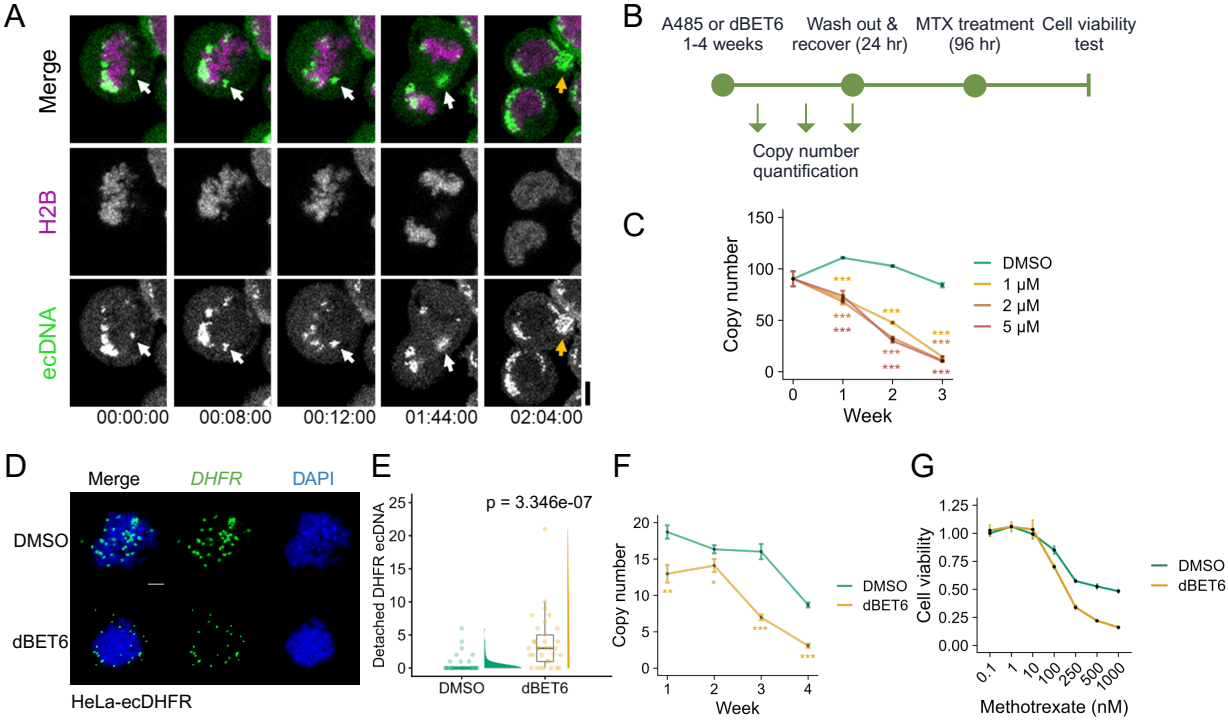
A
Merge
H2B
ecDNA
00:00:00
00:08:00
00:12:00
01:44:00
02:04:00
B
A485 or dBET6
1-4 weeks
Wash out &
recover (24 hr)
MTX treatment
(96 hr)
Cell viability
test
Copy number
quantification
C
Copy number
Week
DMSO
1 μM
2 μM
5 μM
D
Merge
DHFR
DAPI
DMSO
dBET6
HeLa-ecDHFR
E
p = 3.346e-07
Detached DHFR ecDNA
DMSO
dBET6
F
Copy number
Week
DMSO
dBET6
G
Cell viability
Methotrexate (nM)
DMSO
dBET6

Figure S1

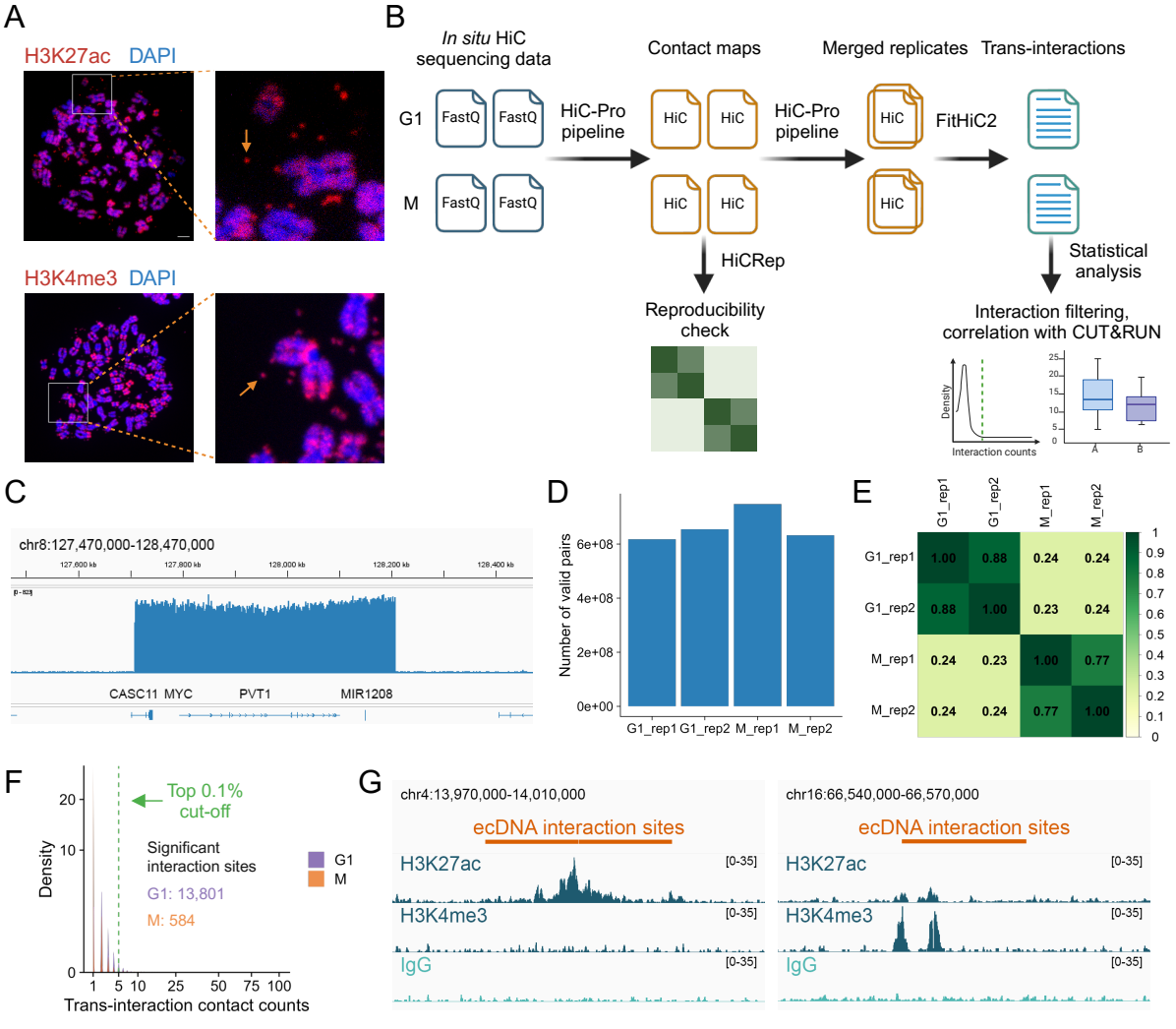
A
H3K27ac DAPI
H3K4me3 DAPI
B
In situ HiC sequencing data
Contact maps
Merged replicates
Trans-interactions
G1
M
FastQ
HiC-Pro pipeline
HiC
FitHiC2
HiCRep
Reproducibility check
Statistical analysis
Interaction filtering, correlation with CUT&RUN
Density
Interaction counts
C
chr8:127,470,000-128,470,000
CASC11 MYC PVT1 MIR1208
D
Number of valid pairs
G1_rep1 G1_rep2 M_rep1 M_rep2
E
G1_rep1 1.00 0.88 0.24 0.24
G1_rep2 0.88 1.00 0.23 0.24
M_rep1 0.24 0.23 1.00 0.77
M_rep2 0.24 0.24 0.77 1.00
F
Top 0.1% cut-off
Significant interaction sites
G1: 13,801
M: 584
Density
Trans-interaction contact counts
G
chr4:13,970,000-14,010,000
chr16:66,540,000-66,570,000
ecDNA interaction sites
H3K27ac
H3K4me3
IgG
[0-35]

Figure S2

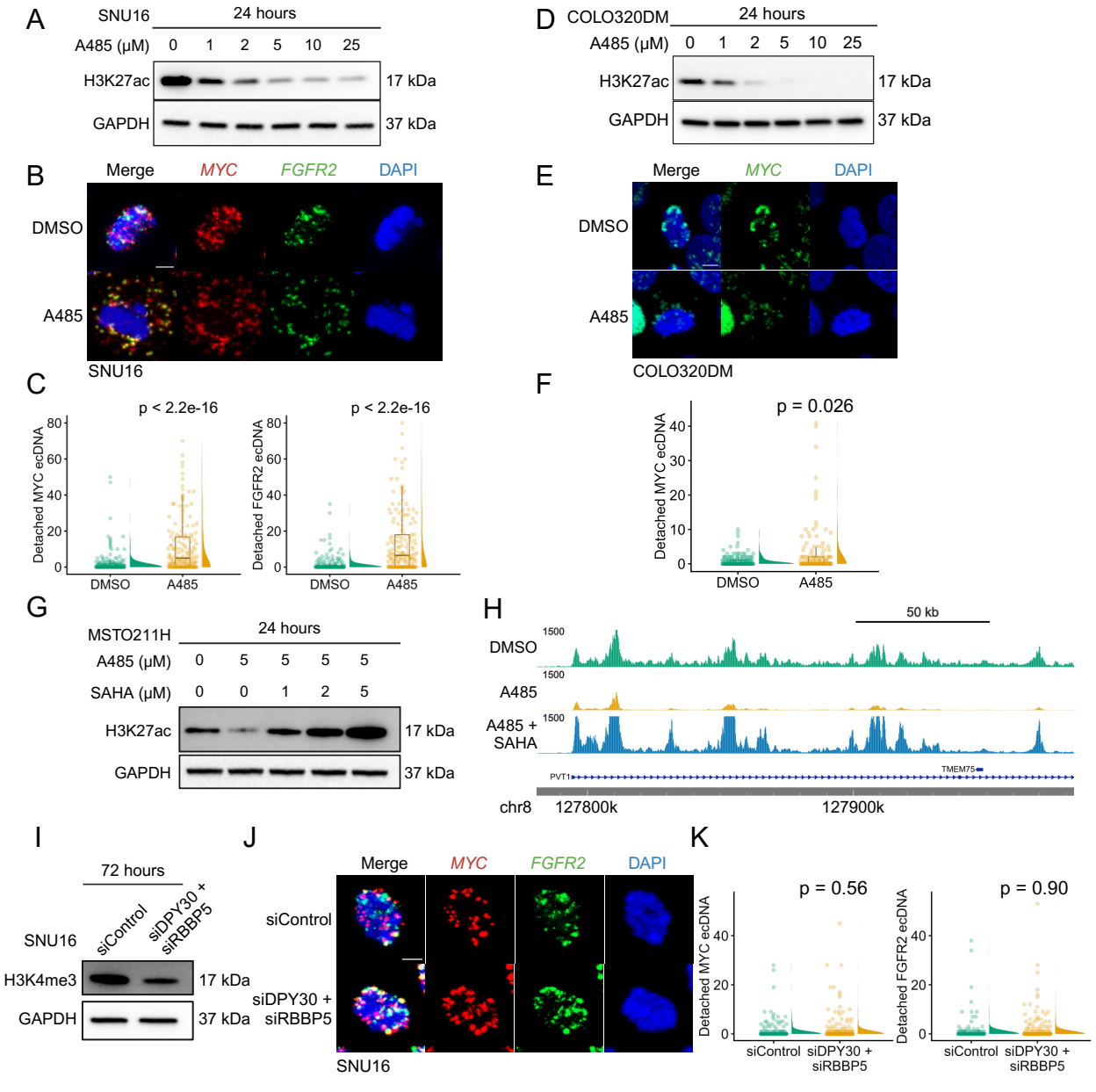
A
SNU16
24 hours
A485 (μM) 0 1 2 5 10 25
H3K27ac
GAPDH
17 kDa
37 kDa
B
Merge
MYC
FGFR2
DAPI
DMSO
A485
SNU16
C
p < 2.2e-16
Detached MYC ecDNA
Detached FGFR2 ecDNA
DMSO
A485
D
COLO320DM
24 hours
A485 (μM) 0 1 2 5 10 25
H3K27ac
GAPDH
17 kDa
37 kDa
E
Merge
MYC
DAPI
DMSO
A485
COLO320DM
F
p = 0.026
Detached MYC ecDNA
DMSO
A485
G
MSTO211H
24 hours
A485 (μM) 0 5 5 5 5
SAHA (μM) 0 0 1 2 5
H3K27ac
GAPDH
17 kDa
37 kDa
H
50 kb
DMSO
A485
A485 + SAHA
1500
PVT1
TMEM75
chr8
127800k
127900k
I
72 hours
SNU16
siControl
siDPY30 + siRBBP5
H3K4me3
GAPDH
17 kDa
37 kDa
J
Merge
MYC
FGFR2
DAPI
siControl
siDPY30 + siRBBP5
SNU16
K
p = 0.56
p = 0.90
Detached MYC ecDNA
Detached FGFR2 ecDNA
siControl
siDPY30 + siRBBP5

Figure S3

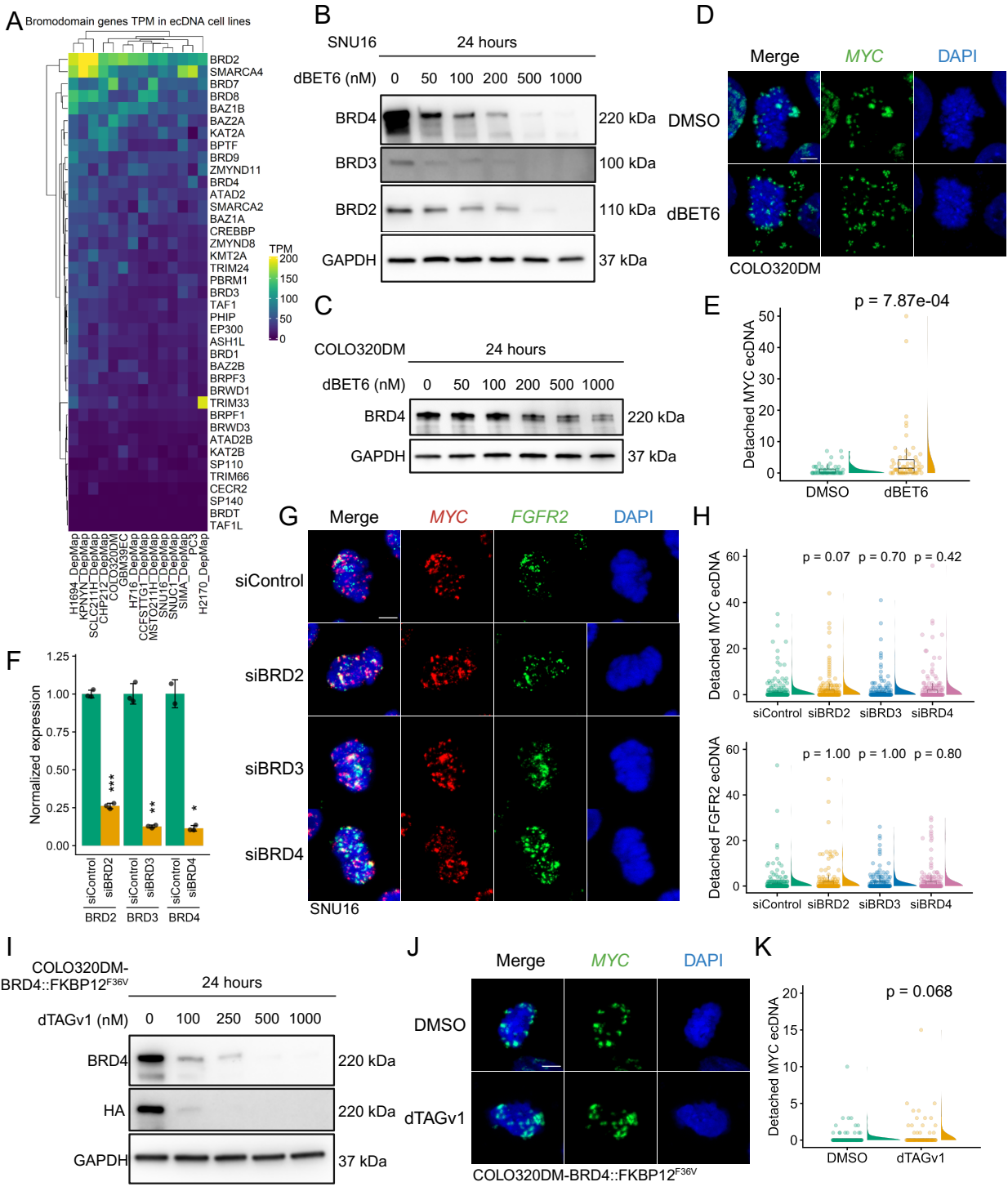
A
Bromodomain genes TPM in ecDNA cell lines
BRD2
SMARCA4
BRD7
BRD8
BAZ1B
BAZ2A
KAT2A
BPTF
BRD9
ZMYND11
BRD4
ATAD2
SMARCA2
BAZ1A
CREBBP
ZMYND8
KMT2A
TRIM24
PBRM1
BRD3
TAF1
PHIP
EP300
ASH1L
BRD1
BAZ2B
BRPF3
BRWD1
TRIM33
BRPF1
BRWD3
ATAD2B
KAT2B
SP110
TRIM66
CECR2
SP140
BRDT
TAF1L
TPM
200
150
100
50
0
H1694_DepMap
KPNYN_DepMap
SCLC21H_DepMap
CHP212_DepMap
COLO320DM
GBM39EC
H716_DepMap
CCFSTTG1_DepMap
MSTO211H_DepMap
SNU16_DepMap
SNU5_DepMap
SIMA_DepMap
PC3
H2170_DepMap
B
SNU16
24 hours
dBET6 (nM) 0 50 100 200 500 1000
BRD4
220 kDa
BRD3
100 kDa
BRD2
110 kDa
GAPDH
37 kDa
C
COLO320DM
24 hours
dBET6 (nM) 0 50 100 200 500 1000
BRD4
220 kDa
GAPDH
37 kDa
D
Merge
MYC
DAPI
DMSO
dBET6
COLO320DM
E
p = 7.87e-04
Detached MYC ecDNA
50
40
30
20
10
0
DMSO
dBET6
F
Normalized expression
1.25
1.00
0.75
0.50
0.25
0.00
***
**
*
siControl
siBRD2
siControl
siBRD3
siControl
siBRD4
BRD2
BRD3
BRD4
G
Merge
MYC
FGFR2
DAPI
siControl
siBRD2
siBRD3
siBRD4
SNU16
H
p = 0.07 p = 0.70 p = 0.42
Detached MYC ecDNA
60
40
20
0
siControl siBRD2 siBRD3 siBRD4
p = 1.00 p = 1.00 p = 0.80
Detached FGFR2 ecDNA
60
40
20
0
siControl siBRD2 siBRD3 siBRD4
I
COLO320DM-BRD4::FKBP12F36V
24 hours
dTAGv1 (nM) 0 100 250 500 1000
BRD4
220 kDa
HA
220 kDa
GAPDH
37 kDa
J
Merge
MYC
DAPI
DMSO
dTAGv1
COLO320DM-BRD4::FKBP12F36V
K
p = 0.068
Detached MYC ecDNA
20
15
10
5
0
DMSO
dTAGv1

Figure S4

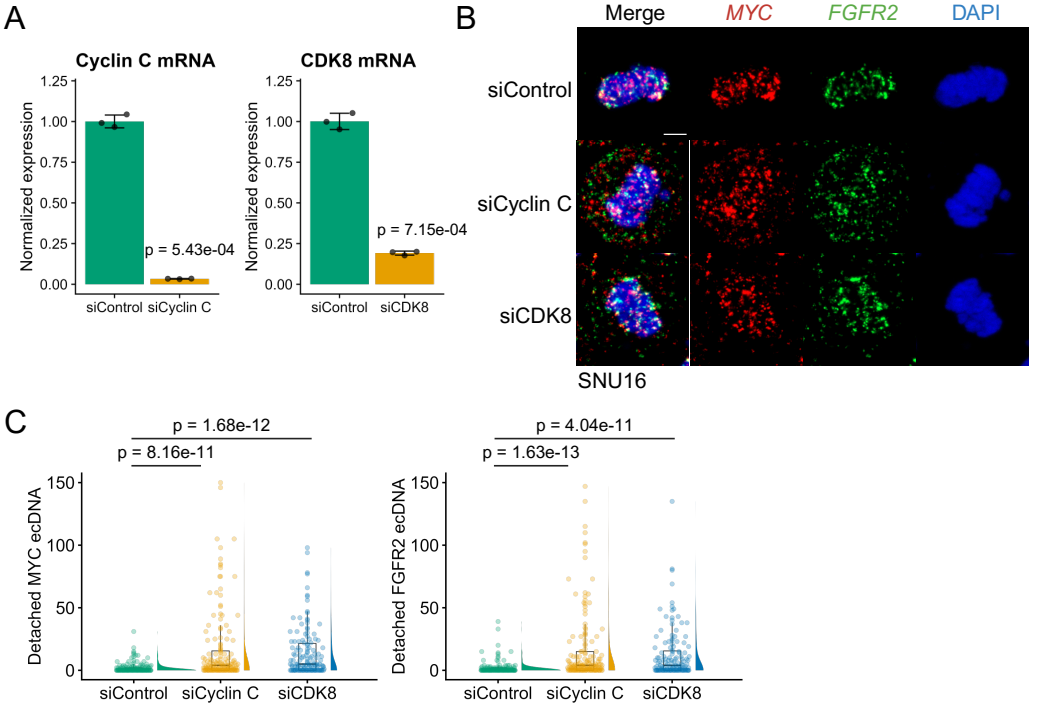
A
Cyclin C mRNA
CDK8 mRNA
Normalized expression
1.25
1.00
0.75
0.50
0.25
0.00
p = 5.43e-04
p = 7.15e-04
siControl
siCyclin C
siCDK8
B
Merge
MYC
FGFR2
DAPI
siControl
siCyclin C
siCDK8
SNU16
C
p = 1.68e-12
p = 8.16e-11
p = 4.04e-11
p = 1.63e-13
Detached MYC ecDNA
Detached FGFR2 ecDNA
150
100
50
0
siControl
siCyclin C
siCDK8

Figure S5

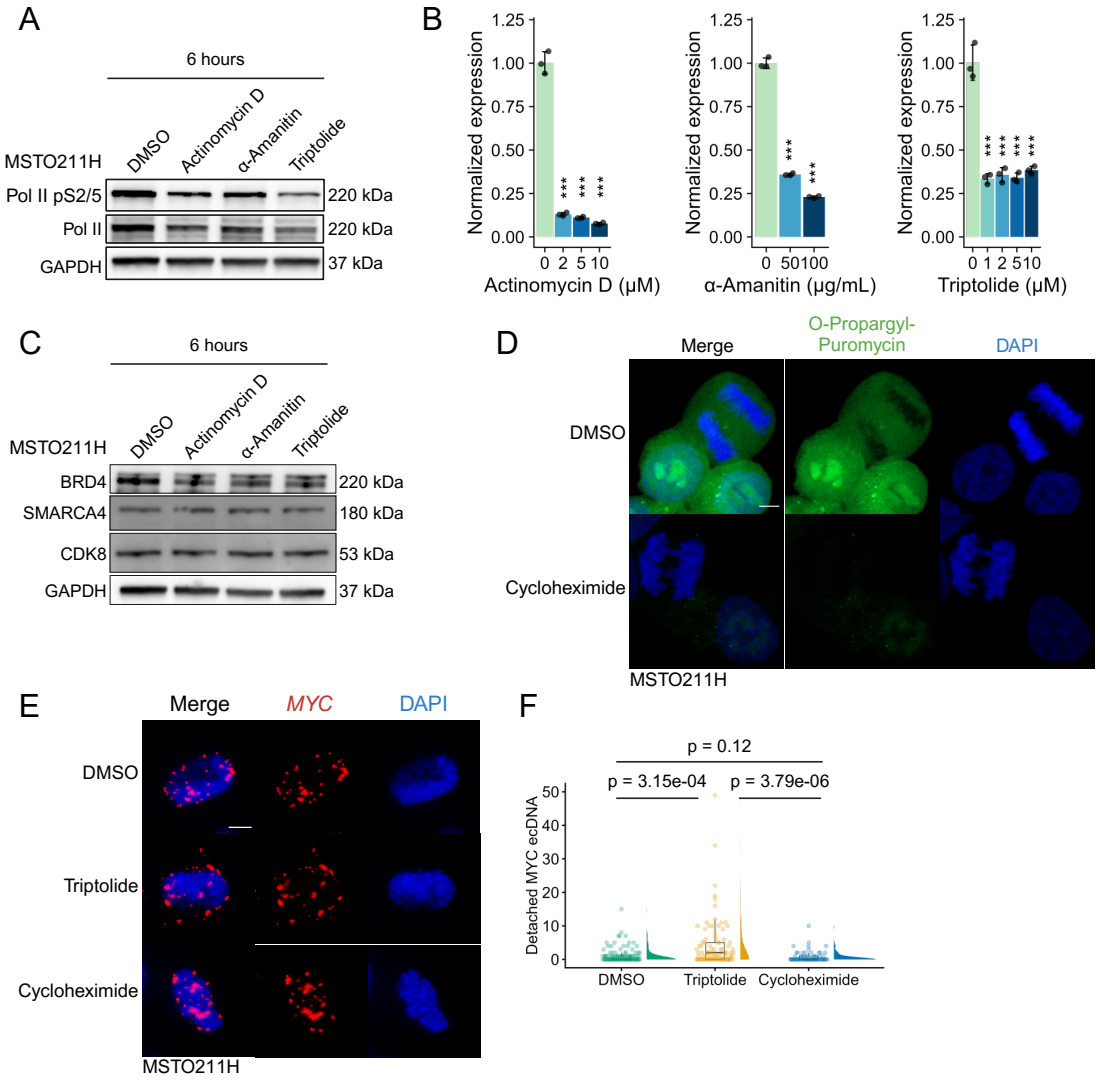
A
6 hours
MSTO211H
DMSO
Actinomycin D
α-Amanitin
Triptolide
Pol II pS2/5
Pol II
GAPDH
220 kDa
220 kDa
37 kDa
B
Normalized expression
1.25
1.00
0.75
0.50
0.25
0.00
***
0 2 5 10
Actinomycin D (μM)
0 50 100
α-Amanitin (μg/mL)
0 1 2 5 10
Triptolide (μM)
C
6 hours
MSTO211H
DMSO
Actinomycin D
α-Amanitin
Triptolide
BRD4
SMARCA4
CDK8
GAPDH
220 kDa
180 kDa
53 kDa
37 kDa
D
Merge
O-Propargyl-Puromycin
DAPI
DMSO
Cycloheximide
MSTO211H
E
Merge
MYC
DAPI
DMSO
Triptolide
Cycloheximide
MSTO211H
F
p = 0.12
p = 3.15e-04
p = 3.79e-06
Detached MYC ecDNA
50
40
30
20
10
0
DMSO
Triptolide
Cycloheximide

Figure S6

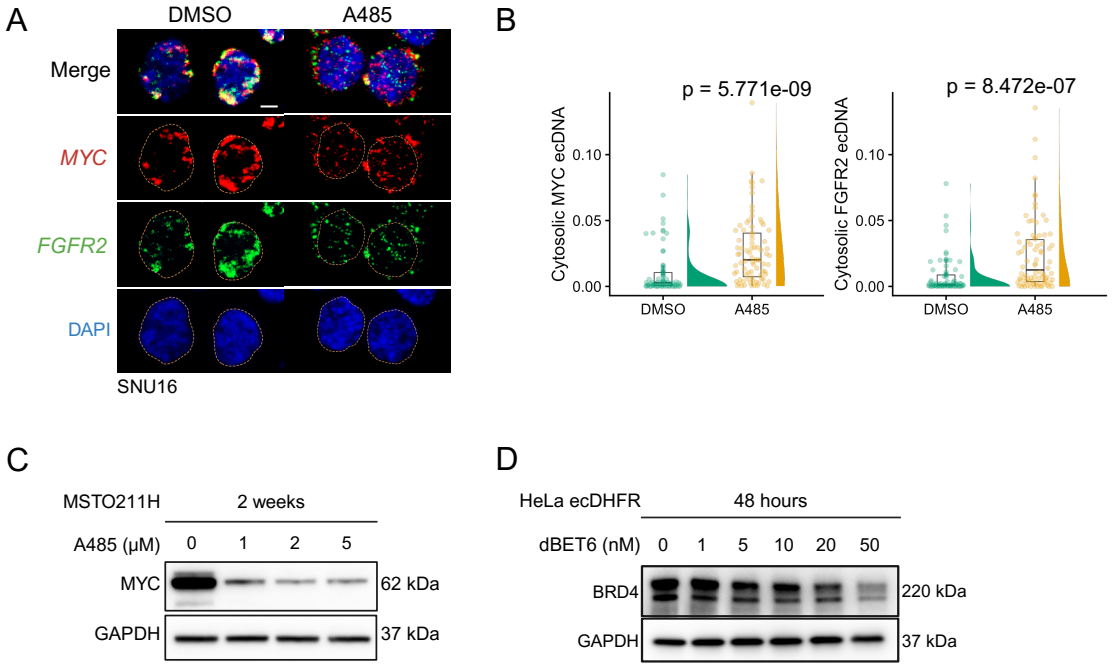
A
DMSO
A485
Merge
MYC
FGFR2
DAPI
SNU16
B
p = 5.771e-09
p = 8.472e-07
Cytosolic MYC ecDNA
Cytosolic FGFR2 ecDNA
0.10
0.05
0.00
DMSO
A485
C
MSTO211H
2 weeks
A485 (μM)
0
1
2
5
MYC
GAPDH
62 kDa
37 kDa
D
HeLa ecDHFR
48 hours
dBET6 (nM)
0
1
5
10
20
50
BRD4
GAPDH
220 kDa
37 kDa